

## Accepted Manuscript

Spectral, thermal, XRD and SEM studies of charge-transfer complexation of hexamethylenediamine and three types of acceptors:  $\pi$ -,  $\sigma$ - and vacant *orbital* acceptors that include quinol, picric acid, bromine, iodine, SnCl<sub>4</sub> and ZnCl<sub>2</sub> acceptors

Abdel Majid A. Adam, Moamen S. Refat, Hosam A. Saad

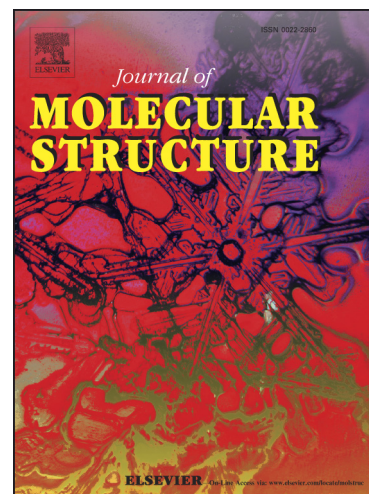
PII: S0022-2860(13)00682-0  
DOI: <http://dx.doi.org/10.1016/j.molstruc.2013.08.006>  
Reference: MOLSTR 19941

To appear in: *Journal of Molecular Structure*

Received Date: 9 March 2013  
Revised Date: 25 July 2013  
Accepted Date: 5 August 2013

Please cite this article as: A.M.A. Adam, M.S. Refat, H.A. Saad, Spectral, thermal, XRD and SEM studies of charge-transfer complexation of hexamethylenediamine and three types of acceptors:  $\pi$ -,  $\sigma$ - and vacant *orbital* acceptors that include quinol, picric acid, bromine, iodine, SnCl<sub>4</sub> and ZnCl<sub>2</sub> acceptors, *Journal of Molecular Structure* (2013), doi: <http://dx.doi.org/10.1016/j.molstruc.2013.08.006>

This is a PDF file of an unedited manuscript that has been accepted for publication. As a service to our customers we are providing this early version of the manuscript. The manuscript will undergo copyediting, typesetting, and review of the resulting proof before it is published in its final form. Please note that during the production process errors may be discovered which could affect the content, and all legal disclaimers that apply to the journal pertain.



**Spectral, thermal, XRD and SEM studies of charge-transfer complexation of hexamethylenediamine and three types of acceptors:  $\pi$ -,  $\sigma$ - and vacant *orbital* acceptors that include quinol, picric acid, bromine, iodine, SnCl<sub>4</sub> and ZnCl<sub>2</sub> acceptors**

Abdel Majid A. Adam<sup>a,\*</sup>, Moamen S. Refat<sup>a,b</sup> and Hosam A. Saad<sup>a,c</sup>

<sup>a</sup> Department of Chemistry, Faculty of Science, Taif University, Al-Haweiah, P.O. Box 888, Zip Code 21974, Taif, Saudi Arabia

<sup>b</sup> Department of Chemistry, Faculty of Science, Port Said University, Port Said, Egypt

<sup>c</sup> Department of Chemistry, Faculty of Science, Zagazig University, Zagazig, Egypt

**Abstract**

In this work, structural, thermal, morphological and pharmacological characterization was performed on the interactions between a hexamethylenediamine (HMDA) donor and three types of acceptors to understand the complexation behavior of diamines. The three types of acceptors include  $\pi$ -acceptors (i.e., quinol (QL) and picric acid (PA)),  $\sigma$ -acceptors (i.e., bromine and iodine) and vacant *orbital* acceptors (i.e., tin(IV) tetrachloride (SnCl<sub>4</sub>) and zinc chloride (ZnCl<sub>2</sub>)). The characterization of the obtained CT complexes was performed using elemental analysis, infrared (IR), Raman, <sup>1</sup>H NMR and electronic absorption spectroscopy, powder X-ray diffraction (XRD) and thermogravimetric (TG) analysis. Their morphologies were studied using scanning electron microscopy with energy-dispersive X-ray analysis (SEM-EDX). The biological activities of the obtained CT complexes were tested for their antibacterial activities. The complex containing the QL acceptor exhibited a remarkable electronic spectrum with a strong, broad absorption band, which had an observed  $\lambda_{\max}$  that was at a much longer wavelength than those of the free reactants. In addition, this complex exhibited strong antimicrobial activities against various bacterial and fungal strains compared to standard drugs. The complexes containing the PA, iodine, Sn(IV) and Zn(II) acceptors exhibited good thermal stability up to 240, 330, 275 and 295 °C, respectively. The complexes containing bromine, Sn(IV) and Zn(II) acceptors exhibited good crystallinity. In addition to its good crystallinity properties, the complex containing the bromine acceptor exhibits a remarkable morphology feature.

**Key words:** Hexamethylenediamine, Charge-transfer interaction, XRD, Morphology, Thermal analysis.

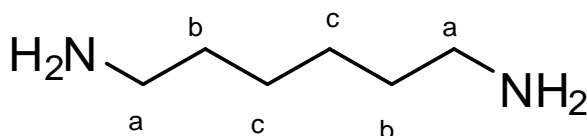
\* Tel: +966502099808.

E-mail address: majidadam@yahoo.com

## 1. Introduction

The chemical and physical properties of electron donor-acceptor (EDA) or charge-transfer (CT) complexes formed by the reaction of  $\pi$ - and  $\sigma$ -electron acceptors with different donors containing nitrogen, sulfur and oxygen atoms, as well as amines, polysulfur and crown ether bases in solution and in the solid state have attracted considerable attention and growing importance in recent years [1-5]. This attention is due to the important role of charge-transfer (CT) complexes in biological systems as well as the significant physical properties of the CT complexes including electrical conductivity and their applications in electronic and solar cells, organic semiconductor lasers, high efficiency non-linear optical materials and organic light emitting diodes (OLEDs). Such complexes also find important applications in the quantitative determination of drugs in pharmaceutical preparations [6-9]. In addition, literature shows that the CT complexes exhibit potential antimicrobial properties against Gram-positive and Gram-negative bacteria as well as fungi [10].

Nitrogen bases are generally of special interest as electron donors because they can function as  $n$ - and  $\pi$ -donors. To shed light on the role of nitrogen bases as significant donors, we have previously investigated the CT complexation properties of tetramethylethylenediamine with various acceptors [11]. Based on the interesting results obtained for the complexation properties of this diamine, we are interested in further investigating diamine compounds. Therefore, as a continuation of our earlier work, we report the synthesis and characterization of six new CT complexes of hexamethylenediamine (HMDA) with quinol (QL), picric acid (PA), bromine, iodine, tin(IV) tetrachloride ( $\text{SnCl}_4$ ) and zinc chloride ( $\text{ZnCl}_2$ ). These complexes were structurally, thermally, morphologically and pharmacologically characterized via elemental analysis, infrared (IR), Raman,  $^1\text{H}$  NMR and electronic absorption spectroscopy, powder X-ray diffraction, thermal analysis and scanning electron microscopy (SEM) as well as with biological applications to study antimicrobial activities.



**Formula I.** Chemical Structure of Hexamethylenediamine.

## 2. Experimental methods

### 2.1 Chemicals and standard stock solutions

All of the chemicals used were of high reagent grade. Hexamethylenediamine (HMDA; Hexane-1,6-diamine,  $C_6H_{16}N_2$ ) and the quinol (QL), picric acid (PA), bromine, iodine,  $SnCl_4$  or  $ZnCl_2$  acceptors were purchased from the Aldrich and Merck Chemical Companies and were used without further purification. Stock solutions of the HMDA and each acceptor at a concentration of  $5.0 \times 10^{-3}$  M were freshly prepared prior to each series of measurements by dissolving precisely weighed quantities in the appropriate volume of the methanol or chloroform solvent. The stock solutions were protected from light.

### 2.2 Instrumentation

The elemental analyses of the carbon, hydrogen and nitrogen content were performed using the microanalysis unit at Cairo University, Egypt, on a Perkin-Elmer CHN 2400 (USA). The electronic absorption spectra of the HMDA donor, the acceptors (QL, PA, bromine and iodine) and the prepared CT complexes were recorded in methanol or chloroform over a wavelength range of 200-800 nm using a Perkin-Elmer Lambda 25 UV/Vis double-beam spectrophotometer at Taif University, Saudi Arabia. The instrument was fitted with a quartz cell that had a path length of 1.0 cm. The infrared (IR) spectra using KBr discs within the range of  $4000-400\text{ cm}^{-1}$  for the solid CT complexes were recorded on a Shimadzu FT-IR spectrophotometer with 30 scans at  $2\text{ cm}^{-1}$  resolution. The Raman laser spectra of the solid CT complexes were measured on a Bruker FT-Raman spectrophotometer equipped with a 50 mW laser at Taif University, Saudi Arabia. The  $^1H$  NMR spectra were recorded by the Analytical Center at the King Abdul Aziz University, Saudi Arabia, on a Bruker DRX-250 spectrometer operating at 250.13 MHz with a dual 5 mm probe head. The measurements were performed at ambient temperature using  $CDCl_3$  as the solvent and TMS (tetramethylsilane) as the internal reference. The  $^1H$  NMR data are expressed in parts per million (ppm) and are internally referenced to the residual proton impurity in the  $CDCl_3$  solvent. The thermogravimetric analysis (TGA) was performed under a static air atmosphere to a temperature of  $800\text{ }^\circ\text{C}$  at a heating rate of  $10\text{ }^\circ\text{C}/\text{min}$  using a Shimadzu TGA-50H thermal analyzer in the Central Lab at the Ain Shams University, Egypt. The X-ray diffraction patterns for the obtained CT complexes were collected on a PANalytical X'Pert PRO X-ray powder diffractometer in the Central Lab at the Ain Shams University, Egypt. The instrument was equipped with a Ge(III) secondary monochromator, and a copper  $K\alpha_1$  X-ray source with a wavelength of 0.154056 nm was employed. The scanning electron microscopy (SEM) images and energy-dispersive X-ray detection (EDX) were recorded with Jeol JSM-6390 equipment at Taif University, Saudi Arabia. The instrument was operated at an accelerating voltage of 20 kV.

### 2.3 Procedures

#### 2.3.1 Synthesis of HMDA CT complexes procedure

The solid HMDA CT complexes with the QL, PA, bromine, iodine,  $SnCl_2$  or  $ZnCl_2$  acceptor were prepared by mixing 1 mmol of the HMDA donor in pure-grade methanol (10 ml) with 1 mmol of each acceptor in methanol (10 ml) (the bromine and iodine were dissolved in chloroform). The solutions were stirred for approximately 20 min and allowed to evaporate slowly at room temperature resulting in the precipitation of the solid CT complexes. The resultant complexes were filtered and

washed well with methanol or chloroform. Then, the synthesized complexes were collected and dried under vacuum over anhydrous calcium chloride for 24 h.

### 2.3.2 Spectrophotometric titration procedure

The spectrophotometric titrations of the detectable CT bands at 341, 342, 295 and 370 nm were performed for the reactions of HMDA with QL, PA, bromine and iodine acceptors as follows: 0.25, 0.50, 0.75, 1.00, 1.50, 2.0, 2.50, 3.00, 3.50 or 4.00 ml of a standard solution ( $5.0 \times 10^{-4}$  M) of the appropriate acceptor in methanol or chloroform was added to 1.00 ml of  $5.0 \times 10^{-4}$  M HMDA, which was also dissolved in the same solvent. The final volume of the mixture was 5 ml. The concentration of HMDA ( $C_d$ ) was maintained at  $5.0 \times 10^{-4}$  M, whereas the concentration of the acceptors ( $C_a$ ) varied from  $0.25 \times 10^{-4}$  M to  $4.00 \times 10^{-4}$  M to produce solutions with a donor: acceptor molar ratio that varied from 4:1 to 1:4. The stoichiometry of the HMDA CT complexes was obtained from the determination of the conventional spectrophotometric molar ratio according to previously published protocols [12] using a plot of the absorbance of each CT complex as a function of the  $C_d:C_a$  ratio. The Benesi–Hildebrand plots [13,14] were constructed to calculate the formation constant ( $K_{CT}$ ) and the absorptivity ( $\epsilon_{CT}$ ) for each CT complex.

### 2.3.3 Pharmacology analyses procedures

#### Antibacterial activity

The antibacterial activity of the prepared HMDA CT complexes and the pure solvent was tested *in vitro* against two Gram-positive bacteria (i.e., *Staphylococcus aureus* (MSSA 22) and *Bacillus subtilis* (ATCC 6051)) and two Gram-negative bacteria (i.e., *Escherichia coli* (K 12) and *Pseudomonas aeruginosa* (MTCC 2488)) using the modified Bauer–Kirby disc diffusion method [15]. The microanalysis facility at Cairo University, Egypt performed the investigations. Briefly, 100  $\mu$ l of the test bacteria were grown in 10 ml fresh medium until they reached a count of approximately  $10^8$  cells/ml for bacteria or  $10^5$  cells/ml for fungi [16]. Then, a 100  $\mu$ l microbial suspension was spread onto agar plates. The nutrient agar medium for the antibacterial tests consisted of 0.5% peptone, 0.1% beef extract, 0.2% yeast extract, 0.5% NaCl and 1.5% agar-agar [17]. Isolated colonies of each organism that may play a pathogenic role were selected from the primary agar plates and tested for susceptibility. After the plates were incubated for 48 h at 37 °C, the inhibition (sterile) zone diameters (including the disc) were measured using slipping calipers from the National Committee for Clinical Laboratory Standards (NCCLS, 1993) [18] and are expressed in mm. The screening was performed using 100  $\mu$ g/ml CT complex. An antibiotic disc containing tetracycline (30  $\mu$ g/disc, Hi-Media) was employed as the positive control. A filter disk impregnated with 10  $\mu$ L of solvent (distilled water, chloroform, DMSO) was employed as the negative control.

#### Antifungal activity

The present HMDA CT complexes were also screened for their antifungal property against *Aspergillus flavus* (laboratory isolate) and *Candida albicans* (IQA-109) in DMSO using the modified Bauer–Kirby disc diffusion method [15]. The complex was dissolved in DMSO. The medium for the antifungal tests consisted of 3% sucrose, 0.3%  $\text{NaNO}_3$ , 0.1%  $\text{K}_2\text{HPO}_4$ , 0.05% KCl, 0.001%  $\text{FeSO}_4$  and 2% agar-agar [17]. The disc diffusion method for the filamentous fungi was tested using the approved standard method (M38-A) [19] developed by the NCCLS for evaluating the

susceptibility of filamentous fungi to antifungal agents. The disk diffusion method for yeast, which was developed as the standard method (M44-P) by the NCCLS, was employed [20]. The plates inoculated with filamentous fungi or yeast were incubated for 48 h at 25 °C or 30 °C, respectively. The antifungal activity of the CT complexes was compared with that of amphotericin B (30 µg/disc, Hi-Media), which was used as the standard antifungal agent (positive control). A filter disk impregnated with 10 µL of solvent (distilled water, chloroform, DMSO) was employed as the negative control. The antifungal activity was determined by measuring the diameters of the sterile zone (mm) in triplicate.

### 3. Results and discussion

#### 3.1 Analytical results

The analytical data, elemental analysis (C, H and N), molar ratio and color of the HMDA CT complexes are shown in Table 1. The elemental analysis data for the prepared CT complexes are in agreement with the molar ratio obtained from the spectrophotometric titrations. The resulting elemental analysis values are in good agreement with the calculated values. The stoichiometry of the HMDA CT complexes with the PA, bromine and iodine acceptors was found to have a 1:2 ratio, whereas its complexes with the QL, SnCl<sub>4</sub> and ZnCl<sub>2</sub> acceptors was found to have a 1:1 ratio. Based on the obtained data, the prepared HMDA CT complexes were formulated as [(HMDA)(QL)], [(HMDA)(PA)<sub>2</sub>], [HMDA]·2Br<sub>2</sub>, [HMDA-I]<sup>+</sup>I<sub>3</sub><sup>-</sup>, [(HMDA)(SnCl<sub>4</sub>)] and [(HMDA)(ZnCl<sub>2</sub>)]. The formation of 1:1 or 1:2 complexes was strongly supported by IR, <sup>1</sup>H NMR and thermal analysis. The QL, PA, bromine and iodine CT complexes have a pale brown, orange, orange yellow and reddish brown color, respectively, but the SnCl<sub>4</sub> and ZnCl<sub>2</sub> complexes are white powders.

#### 3.2 Electronic absorption spectra

##### 3.2.1 Characteristics of the CT bands

Figure 1 shows the electronic absorption spectra of the reactants, HMDA (5.0×10<sup>-4</sup> M) and acceptors (QL, PA, bromine and iodine) (5.0×10<sup>-4</sup>), along with those of the prepared CT complexes. These spectra revealed the presence of the absorption bands that correspond to the CT interactions. These bands are observed at 341, 342, 295 and (275 and 370) nm for the [(HMDA)(QL)], [(HMDA)(PA)<sub>2</sub>], [HMDA]·2Br<sub>2</sub> and [HMDA-I]<sup>+</sup>I<sub>3</sub><sup>-</sup> complexes, respectively. The absorption spectrum of HMDA has a λ<sub>max</sub> at 293 nm, while that of the QL acceptor is 294 nm. Interestingly, when HMDA and QL are mixed together, a new broad band appears at a much longer wavelength (341 nm). This longer wavelength is indicative of charge-transfer. The spectrum of the [HMDA-I]<sup>+</sup>I<sub>3</sub><sup>-</sup> complex contains two new strong absorption bands at 275 and 370 nm. These new bands do not exist in the spectra of the reactants.

##### 3.2.2 Stoichiometry of the HMDA CT complexes

The stoichiometry of the HMDA CT complexes formed between the HMDA donor and the acceptors was determined by the molar ratio method. The peak absorbance values that appeared in the spectra assigned to the prepared CT complexes were measured and plotted as a function of the C<sub>d</sub>:C<sub>a</sub> ratio according to a previously published protocol. Representative spectrophotometric titration plots based on these characterized absorption bands are shown in Figure 2. Based on this figure, the complex formation occurred with a ratio (HMDA: acceptor) of 1:1 for the QL

acceptor and 1:2 for the PA, bromine and iodine acceptors. These stoichiometry values are consistent with the elemental analyses.

### 3.2.3 Determination of the formation constant and the molar extinction coefficient

The formation constant and the molar extinction coefficient of the CT complexes were determined spectrophotometrically using the Benesi–Hildebrand equations. The 1:1 Benesi–Hildebrand equation (Eq. (1)) was employed to calculate the formation constant ( $K_{CT}$ ) and the extinction coefficients ( $\varepsilon$ ) of the HMDA complex with the QL acceptor:

$$(C_a C_d)/A = 1/K\varepsilon + (C_a + C_d)/\varepsilon \quad (1)$$

where  $C_a$  and  $C_d$  are the initial concentrations of the acceptor (QL) and the donor (HMDA), respectively, and  $A$  is the absorbance of the strongly detected CT band at 341 nm. By plotting the  $(C_a C_d)/A$  values as a function of the corresponding  $(C_a + C_d)$  values for this complex, a straight line was obtained, which supports the formation of a 1:1 complex. In the plot, the slope and intercept equal  $1/\varepsilon$  and  $1/K\varepsilon$ , respectively. The Benesi–Hildebrand plot is shown in Figure 3, and the  $K_{CT}$  and  $\varepsilon$  values associated with this complex are given in Table 2.

The 1:2 modified Benesi–Hildebrand equation (Eq. (2)) was employed to calculate the formation constant ( $K_{CT}$ ) and the molar extinction coefficients ( $\varepsilon$ ) of the HMDA complex with the PA, bromine and iodine acceptors:

$$(C_a)^2 C_d/A = 1/K\varepsilon + 1/\varepsilon C_a (4C_d + C_a) \quad (2)$$

where  $C_a$  and  $C_d$  are the initial concentrations of the acceptor (PA, bromine and iodine) and the donor (HMDA), respectively, and  $A$  is the absorbance of the strongly detected CT band. By plotting the  $(C_a)^2 C_d/A$  values for the 1:2 CT complex as a function of the corresponding  $C_a (4C_d + C_a)$  values, a straight line is obtained with a slope of  $1/\varepsilon$  and an intercept at  $1/K\varepsilon$ . The modified Benesi–Hildebrand plots are shown in Figure 3, and the obtained  $K_{CT}$  and  $\varepsilon$  values associated with the PA, bromine and iodine complexes are given in Table 2.

In general, the 1:2 complexes exhibit high values for the formation constants ( $K_{CT}$ ). These high  $K_{CT}$  values reflect the high stabilities of the prepared HMDA CT complexes due to the strong donation of the HMDA donor, which contains two nitrogen atoms. These high values suggest that the prepared CT complexes can be classified as strong [21]. The linearity of the Benesi–Hildebrand plots ( $r > 0.99$ ) further supports this result. The formation constant ( $K_{CT}$ ) is strongly dependent on the nature of the acceptor including the type of electron withdrawing substituents on it (e.g., nitro and halo groups). The results revealed that the [(HMDA)(PA)<sub>2</sub>] complex exhibits a higher  $K_{CT}$  value compared to the other complexes reflecting the relatively higher electron acceptance ability of PA, which contains three nitro groups. The data also revealed that the [(HMDA)(PA)<sub>2</sub>] complex exhibits a very high  $\varepsilon$  value. The  $\varepsilon$  values of the HMDA CT complexes decrease in the following order: [(HMDA)(PA)<sub>2</sub>] > [HMDA]·2Br<sub>2</sub> > [(HMDA)(QL)] > [HMDA-I]<sup>+</sup>I<sub>3</sub><sup>-</sup>.

### 3.2.4 Determination of the spectroscopic and physical data

The spectroscopic and physical data, such as the energy of the CT complex ( $E_{CT}$ ), the oscillator strength ( $f$ ), the transition dipole moment ( $\mu$ ) and the standard free energy ( $\Delta G^\circ$ ), were estimated for the formed CT complexes dissolved in methanol or chloroform at 25 °C. The calculations are summarized below.

The energy values of the CT complexes ( $E_{CT}$ ) of the  $n \rightarrow \pi^*$  and  $\pi \rightarrow \pi^*$  interactions between the HMDA donor and the acceptors were calculated using the equation derived by Briegleb [22]:

$$E_{CT} = (h\nu_{CT}) = 1243.667/\lambda_{CT} \text{ (nm)} \quad (3)$$

where  $\lambda_{CT}$  is the wavelength of the complexation band.

The oscillator strength ( $f$ ) is a dimensionless quantity used to express the transition probability of the CT band. From the CT absorption spectra, the oscillator strength ( $f$ ) can be obtained using the approximate formula [23]:

$$f = 4.319 \times 10^{-9} \int \varepsilon_{CT} d\nu \quad (4)$$

where  $\int \varepsilon_{CT} d\nu$  is the area under the curve of the extinction coefficient of the absorption band in question plotted as a function of the frequency. To a first approximation,

$$f = 4.319 \times 10^{-9} \varepsilon_{CT} \nu_{1/2} \quad (5)$$

where  $\varepsilon_{CT}$  is the maximum extinction coefficient of the CT band and  $\nu_{1/2}$  is the half-bandwidth (i.e., the bandwidth at half of the maximum extinction coefficient value) in  $\text{cm}^{-1}$ .

The transition dipole moments ( $\mu$ ) of the HMDA CT complexes are calculated from Eq. (6) [24]:

$$\mu \text{ (Debye)} = 0.0958 [\varepsilon_{CT} \nu_{1/2} / \nu_{max}]^{1/2} \quad (6)$$

The transition dipole moment ( $\mu$ ) can be employed to determine if a particular transition is allowed. The transition from a bonding  $\pi$  orbital to an antibonding  $\pi^*$  orbital is allowed because the integral that defines the transition dipole moment is nonzero.

The standard free energy changes of complexation ( $\Delta G^\circ$ ) for each complex were calculated from the formation constants using Eq. [25]:

$$\Delta G^\circ = -2.303RT \log K_{CT} \quad (7)$$

where  $\Delta G^\circ$  is the standard free energy change of the CT complexes ( $\text{kJ mol}^{-1}$ ),  $R$  is the gas constant ( $8.314 \text{ J mol}^{-1} \text{ K}^{-1}$ ),  $T$  is the absolute temperature in Kelvin, and  $K_{CT}$  is the formation constant of the complex ( $\text{L mol}^{-1}$ ) at room temperature.

The calculated values of the spectroscopic and physical data for the HMDA CT complexes deduced from Equations 3-7 are presented in Table 2. First, the [(HMDA)(PA)<sub>2</sub>] complex exhibits a considerably higher value for both the oscillator strength ( $f$ ) and the transition dipole moment ( $\mu$ ), which indicates a strong interaction between the donor-acceptor pairs (HMDA and PA) with relatively high probabilities for CT-transitions [26]. Secondly, the obtained values of the standard free energy change ( $\Delta G^\circ$ ) for [HMDA-I]<sup>+</sup><sub>3</sub><sup>-</sup>, [(HMDA)(PA)<sub>2</sub>], [(HMDA)]·2Br<sub>2</sub>, [(HMDA)(QL)] are -48.6, -44.9, -44.8 and -34.9  $\text{kJ mol}^{-1}$ , respectively. These negative values indicate that the interaction between the HMDA and the acceptors is spontaneous [27].

### 3.3 Interpretation of the IR spectra

The infrared absorption spectra of the HMDA solid CT complexes were recorded in the frequency range 4000-400  $\text{cm}^{-1}$  using a KBr disc, and their characteristic bands are provided in Table 3. The full IR spectra of the HMDA CT complexes are shown in Figure 4. The IR spectrum of HMDA contains the following characteristic absorption bands: (i) 3339  $\text{cm}^{-1}$ , which was assigned to the stretching vibrational band of (N-H); (ii) 2934 and 2856  $\text{cm}^{-1}$ , which were assigned to the asymmetric and symmetric stretching vibrational bands of  $-\text{CH}_2$ , respectively; (iii) 1660  $\text{cm}^{-1}$ , which corresponds to the bending deformation bands of N-H; (iv) the bending deformation bands of  $-\text{CH}_2$  are assigned to the bands at 1476, 1455, 1395

and  $1360\text{ cm}^{-1}$ ; (v) the asymmetric and symmetric stretching bands (i.e.,  $\nu_{\text{as}}(\text{C-N}) + \nu_{\text{s}}(\text{C-N})$ ) of C-N appear at  $1284$  and  $1237\text{ cm}^{-1}$  and  $1061$  and  $1014\text{ cm}^{-1}$ , respectively; (vi) both rocking  $\delta(\text{NH})$  and in-plane bending  $\delta(\text{CH})$  have detectable bands at  $970$  and  $878\text{ cm}^{-1}$  and  $823$  and  $733\text{ cm}^{-1}$ , respectively; and (vii) the band at  $611\text{ cm}^{-1}$  is assigned to the out-of-plane bending of  $\delta(\text{C-N})$ . The IR spectra of the prepared CT complexes showed significant changes compared to that of the HMDA donor, which indicated complexation between the HMDA donor and the acceptors. However, the bands associated with the prepared CT complexes exhibit variation in their intensities and, in some cases, show small shifts in the frequency values compared to those of the free acceptor and HMDA donor. This variation could be due to symmetry and electronic structure changes in both the acceptor and HMDA in the prepared CT complexes compared to those of the free molecules. In the IR spectra, the [(HMDA)(QL)] and [(HMDA)(PA)<sub>2</sub>] complexes are characterized by the appearance of absorption bands at  $3267\text{ cm}^{-1}$  for the QL complex and at  $3240\text{ cm}^{-1}$  for the PA complex. These absorption bands do not appear in the spectra of the free HMDA donor or those of the QL and PA acceptors. These broadened peaks can be attributed to the stretching vibration of the intermolecular hydrogen bond formed through the proton transfer phenomena from the acidic center of each acceptor (QL and PA) to the lone pair of electrons on the nitrogen as dictated by acid–base theory [28-30]. As expected, the characteristic IR bands of the HMDA donor in the [HMDA]·2Br<sub>2</sub> and [HMDA-I]<sup>+</sup>I<sub>3</sub><sup>-</sup>, [(HMDA)(SnCl<sub>4</sub>)] and [(HMDA)(ZnCl<sub>2</sub>)] complexes exhibit small changes in the band intensities and frequency values. In the IR spectra of the [(HMDA)(SnCl<sub>4</sub>)] and [(HMDA)(ZnCl<sub>2</sub>)] complexes, these two complexes exhibited non-ligand bands at  $460$ - $570\text{ cm}^{-1}$ , which were assigned to the  $\nu(\text{M-N})$  vibrations [31].

### 3.4 Interpretation of the laser Raman spectra

Figure 5 shows the representative laser Raman spectra of the HMDA CT complexes. The [(HMDA)(PA)<sub>2</sub>] complex exhibits vibrations at  $1561$  and  $1336\text{ cm}^{-1}$ , which clearly correspond to the symmetric vibrational modes of  $\nu(\text{C=C})$  and the bending deformation of  $\delta(\text{CH})$ , respectively. The  $\nu(\text{C=C})$  vibrational band of the QL acceptor appears at  $1594\text{ cm}^{-1}$  in the Raman spectrum of the [(HMDA)(QL)] complex. Based on the Raman spectra of the [(HMDA)(SnCl<sub>4</sub>)] and [(HMDA)(ZnCl<sub>2</sub>)] complexes, the non-ligand bands occurred at  $570$  and  $292\text{ cm}^{-1}$  and  $315$  and  $168\text{ cm}^{-1}$ , which correspond to the  $\nu(\text{M-N})$  and  $\nu(\text{M-Cl})$  vibrations, respectively [31]. Raman spectroscopy can only provide valuable information on the nature and structural features of polyiodide anions. The laser Raman spectrum of the HMDA-iodine complex contained the characteristic bands for the triiodine (I<sub>3</sub><sup>-</sup>) unit, which was observed at  $164$ ,  $123$  and  $98\text{ cm}^{-1}$  and assigned to  $\nu_{\text{as}}(\text{I-I})$ ,  $\nu_{\text{s}}(\text{I-I})$  and  $\delta(\text{I}_3^-)$ , respectively [32]. Maki and Forneris [33] assigned the lines of the Raman spectra of I<sub>3</sub><sup>-</sup> that occurred at  $111$  and  $161\text{ cm}^{-1}$  to the symmetric and anti-symmetric stretching vibrations, respectively. The observed Raman spectrum confirmed the formation of the [HMDA-I]<sup>+</sup>I<sub>3</sub><sup>-</sup> complex, which was also supported by the electronic absorption spectrum of the iodine complex. The appearance of the two absorption bands at approximately  $370$  and  $275\text{ nm}$  is well known to be characteristic of the formation of the triiodine ion (I<sub>3</sub><sup>-</sup>) [34-36]. However, the I<sub>3</sub><sup>-</sup> ion may be linear (D<sub>h</sub>) or nonlinear (C<sub>2v</sub>). Group theoretical analysis indicates that the I<sub>3</sub><sup>-</sup> has C<sub>2v</sub> symmetry and displays three vibrations including  $\nu_{\text{as}}(\text{I-I})$ , A<sub>1</sub>;  $\nu_{\text{s}}(\text{I-I})$ , B<sub>2</sub>; and  $\delta$ , (I<sub>3</sub><sup>-</sup>); A<sub>1</sub>. All of these

vibrations are IR active, which is in good agreement with the observation of three Raman bands for  $[\text{HMDA-I}]^+\text{I}_3^-$ . According to the above discussion, a general mechanism proposed for the formation of the  $[\text{HMDA-I}]^+\text{I}_3^-$  complex is as follows:



The Raman spectrum for the free bromine exhibited a very intense band at  $310 \text{ cm}^{-1}$  [11]. In the Raman spectrum of the  $[\text{HMDA}] \cdot 2\text{Br}_2$  complex, the halogen vibration band ( $\nu(\text{Br-Br})$ ) is shifted to a lower frequency of  $271 \text{ cm}^{-1}$  upon complexation.

### 3.5 Interpretation of the $^1\text{H}$ NMR spectra

The nuclear magnetic resonance spectra provide evidence of the complexation pathway. The 400 MHz  $^1\text{H}$  NMR spectra of the  $[(\text{HMDA})(\text{QL})]$ ,  $[(\text{HMDA})(\text{PA})]$ ,  $[(\text{HMDA})(\text{SnCl}_4)]$  and  $[(\text{HMDA})(\text{ZnCl}_2)]$  CT complexes were measured in  $\text{CDCl}_3$  at room temperature and are provided in Figure 6. The chemical shifts ( $\delta$ ) of the different types of protons in these CT complexes include the following:

- (1) **HMDA donor**:  $\delta = 1.22$  (s, 4H,  $2\text{NH}_2$ ), 1.36 (t, 4H,  $2\text{CH}_2$ ,  $\text{C}_{(c)}$ ), 1.49 (m, 4H,  $2\text{CH}_2$ ,  $\text{C}_{(b)}$ ), 2.67 (t, 4H,  $2\text{CH}_2$ ,  $\text{C}_{(a)}$ ).
- (2)  **$[(\text{HMDA})(\text{QL})]$  complex**:  $\delta = 1.31$  (t, 4H,  $2\text{CH}_2$ ,  $\text{C}_{(c)}$ ), 1.52 (m, 4H,  $2\text{CH}_2$ ,  $\text{C}_{(b)}$ ), 2.88 (t, 4H,  $2\text{CH}_2$ ,  $\text{C}_{(a)}$ ), 3.17 (b, 4H,  $2\text{NH}_2$ , Hydrogen bonded with quinol OH), 5.23 (s, 2H, Ar-OH, quinol OH protons hydrogen bonded with  $\text{NH}_2$ ), 6.55 (s, 4H, Ar-H of quinol).
- (3)  **$[(\text{HMDA})(\text{PA})_2]$  complex**:  $\delta = 1.31$  (t, 4H,  $2\text{CH}_2$ ,  $\text{C}_{(c)}$ ), 1.51 (m, 4H,  $2\text{CH}_2$ ,  $\text{C}_{(b)}$ ), 2.76 (t, 4H,  $2\text{CH}_2$ ,  $\text{C}_{(a)}$ ), 3.42 (b, 4H,  $2\text{NH}_2$ , Hydrogen bonded with picric acid OH), 7.61 (b, 2H, Ar-OH, picric acid OH protons hydrogen bonded with  $\text{NH}_2$ ), 8.65 (s, 4H, Ar-H of picric acid).
- (4)  **$[(\text{HMDA})(\text{SnCl}_4)]$  complex**:  $\delta = 1.31$  (t, 4H,  $2\text{CH}_2$ ,  $\text{C}_{(c)}$ ), 1.55 (m, 4H,  $2\text{CH}_2$ ,  $\text{C}_{(b)}$ ), 2.74 (t, 4H,  $2\text{CH}_2$ ,  $\text{C}_{(a)}$ ), 3.42 (b, 4H,  $2\text{NH}_2$ ).
- (5)  **$[(\text{HMDA})(\text{ZnCl}_2)]$  complex**:  $\delta = 1.26$  (t, 4H,  $2\text{CH}_2$ ,  $\text{C}_{(c)}$ ), 1.48 (m, 4H,  $2\text{CH}_2$ ,  $\text{C}_{(b)}$ ), 2.63 (t, 4H,  $2\text{CH}_2$ ,  $\text{C}_{(a)}$ ), 3.40 (b, 4H,  $2\text{NH}_2$ ).

The HMDA free donor exhibited four characteristic bands at  $\delta = 1.22$  ppm for the two aliphatic  $-\text{NH}_2$  groups along with three peaks at 1.36, 1.49 and 2.67 ppm corresponding to three different  $\text{CH}_2$  groups (6H;  $6\text{CH}_2$ );  $\text{CH}_2$   $\text{C}_{(c)}$ ,  $\text{CH}_2$   $\text{C}_{(b)}$  and  $\text{CH}_2$   $\text{C}_{(a)}$ , respectively. In the  $[(\text{Qui})(\text{QL})]$  complex, the high upfield shift of the phenolic proton ( $-\text{OH}$ ) band of quinol, which is observed at approximately  $\delta \sim 8.59$  ppm in the spectrum of the QL acceptor [30], to 5.23 ppm as well as a high downfield shift of the  $\text{NH}_2$  band in HMDA ( $\delta = 3.17$  ppm) indicates the involvement of the  $-\text{NH}_2$  groups of the HMDA donor and the ( $-\text{OH}$ ) group of the QL acceptor in chelating the QL acceptor to the HMDA donor via deprotonation. The downfield chemical shift of all of the protons in the  $-\text{CH}_2$  groups is due to the formation of the intermolecular CT complex. In the  $[(\text{HMDA})(\text{PA})_2]$  complex, the high upfield shift of the band associated with the OH proton of picric acid, which is observed at  $\delta = 11.94$  for the free picric acid [37], to 7.61 ppm along with a high downfield shift of the  $\text{NH}_2$  signal of the HMDA ( $\delta = 3.42$  ppm) confirms the formation of intermolecular hydrogen bonds between PA and HMDA [38]. In addition, the electronic environments of the HMDA proton change during the formation of the CT complexes, and the proton signal of the aromatic rings in the PA was shifted slightly downfield from 8.624 (pure PA) to 8.650 ppm after complexation. Based on the  $^1\text{H}$  NMR of the OL and PA complex with HMDA, the complexes are created by the formation of a hydrogen bond

between the N atom of the HMDA and the H atom of the –OH groups in each acceptor. After complexation of [(HMDA)(ZnCl<sub>2</sub>)], the characteristic signal for the –NH<sub>2</sub> protons, which occurs at 1.22 ppm in free HMDA donor, was shifted downfield to 3.4 ppm due to the deshielding effect of the Zn(II) ion. In addition, a small downfield shift in the CH<sub>2</sub> bands was observed. The more positive Sn(IV) cation exhibited a larger deshielding effect in its complex with HMDA, resulting in a larger downfield shift for all of the absorption bands compared to the Zn(II) complex.

### 3.6 Thermal results

To determine the formula and structure of the new HMDA CT complexes, thermogravimetric analysis (TG) was performed for these complexes over a temperature range of 25-800 °C under a static air atmosphere. The TG curves were redrawn with the mg mass loss as a function of temperature. Fig. 7 shows the thermograms for the HMDA CT complexes. Table 4 provides the TG temperature range together with the corresponding weight loss for each step in the decomposition process of these complexes.

The TG curve of the [(HMDA)(QL)] complex indicates that this complex is thermally stable in the 25-100°C temperature range. The decomposition of the complex began at ~100° C and was complete at ~650° C. The thermal decomposition of this complex occurs in three steps within the temperature range of 25-800 °C. The first mass loss step occurs between 25-230° C, which corresponds to the loss of C<sub>2</sub>H<sub>8</sub>N<sub>2</sub> molecules and a weight loss of 26.29%. The second degradation step at 230-514° C is attributed to the loss of C<sub>5</sub>H<sub>4</sub>O<sub>2</sub> molecules, which represents a weight loss of (obs.=42.81, cal.= 42.42%). The last mass loss step occurs between 514-800 °C and corresponds to the loss of C<sub>3</sub>H<sub>10</sub> resulting in a few carbon atoms that remain as a residue. The thermal analysis curve of the [(HMDA)(PA)<sub>2</sub>] complex indicates that decomposition occurs in two decomposition steps within the 25-800 °C temperature range. The first decomposition step in the temperature range of 25-370°C has a weight loss of approximately 70.49% and is attributed to the formation of C<sub>7</sub>H<sub>12</sub>N<sub>8</sub>O<sub>14</sub> molecules. The second decomposition step occurred within the 370-800 °C temperature range and was assigned to the removal of C<sub>11</sub>H<sub>10</sub> molecules. Theoretically, the loss of this moiety corresponds to the loss of 29.51%. The thermal decomposition of the [HMDA]·2Br<sub>2</sub> complex proceeds in three successive degradation steps within the temperature range of 25-800 °C. The decomposition steps occur in the temperature ranges of 25-265, 265-468 and 468-800°C with weight losses of 43.86, 46.8 and 9.34%, which correspond to the loss of Br<sub>2</sub> + 2CH<sub>4</sub>, Br<sub>2</sub> + CH<sub>4</sub> + N<sub>2</sub> and CH<sub>4</sub> + 2CO<sub>2</sub>, respectively. The total percentage of weight loss observed (100%) matched the calculated weight loss of 99.96%. The thermal degradation of the [HMDA-I]<sup>+</sup>I<sub>3</sub><sup>-</sup> complex occurs in two degradation stages within the 25-800 °C temperature range. The mass change begins at ~330°C and continues to 800 °C. The first stage of decomposition occurs within the temperature range of 25-460° C, corresponding to the loss of two iodine molecules with a weight loss of 81.40%, which is in good agreement with the calculated value (81.31%). The second decomposition step occurred in the temperature range of 460-800° C and is assigned to the removal of four methane molecules and one nitrogen molecule. The observed weight loss of 14.75% is in good agreement with the theoretical weight loss value of 14.64%. The decomposition of this organic moiety led to residual carbon atoms as a final product. The TG thermogram of the [(HMDA)(SnCl<sub>4</sub>)] complex indicated that the thermal decomposition of this complex proceeds via one degradation step within

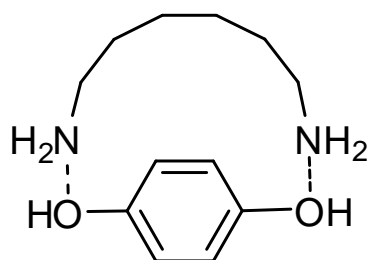
the 25-800 °C temperature range. This decomposition begins at ~ 275 °C, and the observed weight loss associated with this step is 68.52%, which can be attributed to the loss of the C<sub>6</sub>H<sub>16</sub>N<sub>2</sub>Cl<sub>4</sub> moiety and is in excellent agreement with the calculated value of 68.50%. The continuous weight loss in this stage resulted in a residual tin metal remaining as the final fragment. The obtained data indicate that the [(HMDA)(ZnCl<sub>2</sub>)] complex was thermally decomposed in three successive decomposition steps within the temperature range of 25-800 °C. The decomposition steps occurred at 25-367, 367-546 and 546-800°C with a weight loss of 23.71, 36.4 and 14.1%, which corresponds to the loss of C<sub>2</sub>H<sub>8</sub>N<sub>2</sub>, C<sub>4</sub>H<sub>8</sub>Cl and ½Cl<sub>2</sub>, respectively. The final thermal product obtained at 800 °C is zinc metal. These steps are associated with a total weight loss of 74.20%, which is in good agreement with the calculated value (74.05%).

### 3.6 Kinetic results

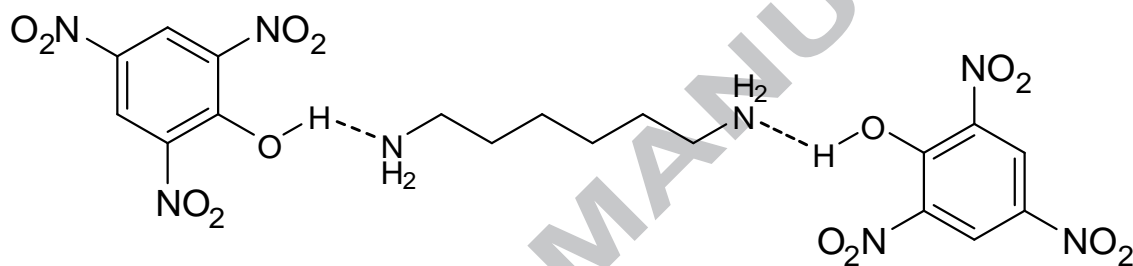
Several equations have been proposed to analyze a TG curve and to obtain the kinetic parameters. Two different methods were employed to evaluate the kinetic thermodynamic parameters: the Coats–Redfern method [39] and the Horowitz–Metzger method [40]. The kinetic thermodynamic parameters (i.e., the activation energy ( $E^*$ ), the frequency factor ( $A$ ), the enthalpy of activation ( $H^*$ ), the entropy of activation ( $S^*$ ) and the free energy of activation ( $G^*$ )) for the decomposition processes of the HMDA CT complexes were evaluated graphically (Figure 8) by employing the Coats-Redfern and Horowitz-Metzger methods, and the evaluated data are listed in Table 5. The activation energy ( $E^*$ ) of the complexes is expected to increase with the increasing thermal stability of complexes. Therefore, the  $E^*$  value for the [(HMDA)(PA)<sub>2</sub>] complex is higher compared to the other complexes, which indicates the higher thermal stability of the [(HMDA)(PA)<sub>2</sub>] complex. By comparing the  $E^*$  values for the main decomposition stage of the HMDA CT complexes, we observed the following trend for the different acceptors: PA > I<sub>2</sub> > Zn(II) > Sn(IV) > QL > Br<sub>2</sub>. These differences may be due to the reactivity of the complexes and the electronic configuration of the acceptor when complexed with the HMDA donor. The calculated  $E^*$  values using the Coats–Redfern and Horowitz–Metzger methods for the main decomposition stage of the complexes are 1×10<sup>6</sup> kJ mol<sup>-1</sup> for [(HMDA)(PA)<sub>2</sub>], 3.1×10<sup>5</sup> kJ mol<sup>-1</sup> for [HMDA-I]<sup>+</sup>I<sub>3</sub><sup>-</sup>, 1.3×10<sup>5</sup> kJ mol<sup>-1</sup> for [(HMDA)(ZnCl<sub>2</sub>)], 8.4×10<sup>4</sup> kJ mol<sup>-1</sup> for [(HMDA)(SnCl<sub>4</sub>)], 4.2×10<sup>4</sup> kJ mol<sup>-1</sup> for [(HMDA)(QL)] and 3.9×10<sup>4</sup> kJ mol<sup>-1</sup> for [HMDA]·2Br<sub>2</sub>. The entropy of activation ( $\Delta S^*$ ) is found to be negative in most cases, which indicates that the decomposition reactions proceed spontaneously. The  $\Delta S^*$  values of the HMDA CT complexes occur in a decreasing order as follows: [(HMDA)(PA)<sub>2</sub>] > [HMDA-I]<sup>+</sup>I<sub>3</sub><sup>-</sup> > [(HMDA)(ZnCl<sub>2</sub>)] > [(HMDA)(SnCl<sub>4</sub>)] > [HMDA]·2Br<sub>2</sub> > [(HMDA)(QL)]. The satisfactory values for the correlation coefficients from the Arrhenius plots of the thermal decomposition steps were observed to be  $r \sim 1$  for all cases, which indicates a good fit with the linear function and reasonable agreement between the experimental data and the kinetic parameters.

### 3.8 Structural interpretation

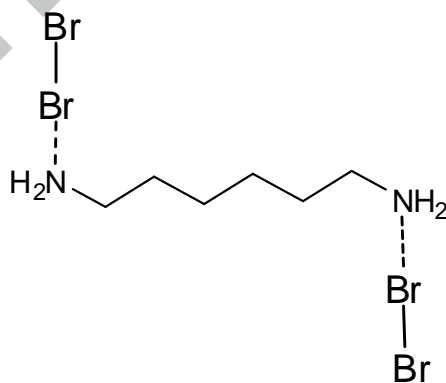
The structures of the CT complexes of the HMDA donor with the QL, PA, Br<sub>2</sub>, I<sub>2</sub>, SnCl<sub>4</sub> or ZnCl<sub>2</sub> acceptors are confirmed by elemental analysis, spectrophotometric titration, IR and <sup>1</sup>H NMR spectra, and thermal analysis. The proposed structures of these CT complexes are shown in Formulas II, III, IV, V, VI and VII.



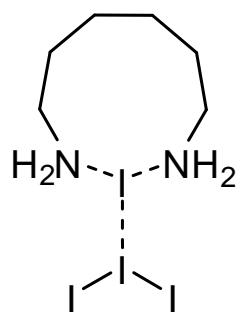
**Formula II.** Proposed structural formula of the [(HMDA)(QL)] complex.



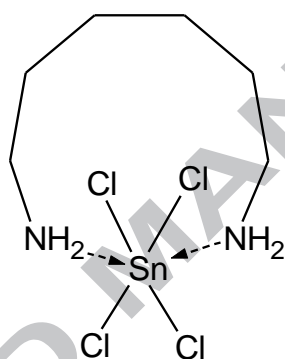
**Formula III.** Proposed structural formula of the [(HMDA)(PA)<sub>2</sub>] complex.



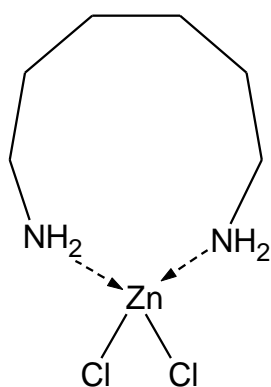
**Formula IV.** Proposed structural formula of the [HMDA]·2Br<sub>2</sub> complex.



**Formula V.** Proposed structural formula of the  $[\text{HMDA-I}]^+\text{I}_3^-$  complex.



**Formula VI.** Proposed structural formula of the  $[(\text{HMDA})(\text{SnCl}_4)]$  complex.



**Formula VII.** Proposed structural formula of the  $[(\text{HMDA})(\text{ZnCl}_2)]$  complex.

### 3.9 XRD characterization

To obtain further evidence regarding the structure of the HMDA CT complexes and to demonstrate their crystallinity, powder X-ray diffraction (XRD) studies were performed using a PANalytical model X'PERT-PRO X-ray powder diffractometer system. The indexed diffractograms obtained in the range of  $5^\circ < 2\theta < 70^\circ$  for these complexes are shown in Figure 9. The particle size of these two complexes was estimated from their XRD patterns based on the highest intensity value compared to the other peaks using the well-known Debye–Scherrer formula given in (Eq. 13) [41].

$$D = K\lambda / \beta \cos \theta \quad (13)$$

where  $D$  is the apparent particle size of the grains,  $K$  is a constant (0.94 for Cu grid),  $\lambda$  is the X-ray wavelength used (1.5406 Å),  $\theta$  is half the scattering angle (the Bragg diffraction angle), and  $\beta$  is the full-width at half-maximum (FWHM) of the X-ray diffraction line (additional peak broadening) in radians. Table 6 presents the XRD spectral data (i.e.,  $2\theta$ ,  $\beta$ ,  $d$  (the interplanar spacing between atoms) and  $D$  in nm) for the [(HMDA)(QL)], [(HMDA)(PA)<sub>2</sub>], [HMDA]·2Br<sub>2</sub>, [(HMDA)(SnCl<sub>4</sub>)] and [(HMDA)(ZnCl<sub>2</sub>)] complexes.

Based on the XRD investigations, the following results were obtained:

- (1) The primary characteristic scattering peak of the [(HMDA)(QL)], [(HMDA)(PA)<sub>2</sub>], [HMDA]·2Br<sub>2</sub>, [(HMDA)(SnCl<sub>4</sub>)] and [(HMDA)(ZnCl<sub>2</sub>)] complex occurred at 21.471°, 28.121°, 32.525°, 9.475° and 9.137° in the diffraction pattern, respectively.
- (2) The XRD patterns of the HMDA CT complexes differ from each other.
- (3) For the complexes with the bromine, Sn(IV) and Zn(IV) acceptors, the appearance of a sharp and strong Bragg peak indicates the formation of a well-defined distorted crystalline structure.
- (4) Using the Debye–Scherrer equation, the particle size values of the complexes were found to be ~4.9, ~7.5, ~10, ~11.6 and ~7.3 nm for the [(HMDA)(QL)], [(HMDA)(PA)<sub>2</sub>], [HMDA]·2Br<sub>2</sub>, [(HMDA)(SnCl<sub>4</sub>)] and [(HMDA)(ZnCl<sub>2</sub>)] complexes, respectively.
- (5) Based on these values, the particle sizes are on the nanoscale.

### 3.10 Morphology characterization

Scanning electron microscopy (SEM) was employed to observe the morphology and particle size of the HMDA CT complexes. The surface images obtained with the SEM technique provide general information regarding the microstructure, surface morphology, particle size, chemical composition, and porous structures of the surfaces. In addition, the chemical compositions of the complexes were determined using energy-dispersive X-ray diffraction (EDX). Figure 10 depicts the SEM photographs of the synthesized HMDA CT complexes along with their EDX spectra. Analyses of the SEM photographs and EDX profiles of the HMDA CT complexes provided the following observations:

- (1) The morphological phases of the synthesized complexes showed a uniform matrix in the SEM images indicating the formation of a homogeneous material.
- (2) The size of the particles differed substantially for each acceptors.
- (3) The particles of the QL complex appear as agglomerates and display a different granule size and shape with a particle size in the range of 10-50 μm.
- (4) The particles of the PA complex are flake-shaped, where most of the particles exhibit angular shapes with estimated sizes in the range of 50-100 μm.

- (5) The complexation of HMDA with bromine leads to a very interesting morphology. The image of the obtained complex shows coherent a rock-like-shaped morphology with a particle of size 10  $\mu\text{m}$ . From the multi SEM photographs with various degrees of enlargement (i.e., x500, x1000, x1500, x2000) (Figure 10C), the particles of this complex have a well-defined morphology, and smaller granules are clearly observed on the surface of each of the larger granules.
- (6) A gelatin-like shape is observed for the iodine complex, which has clearly visible holes and a particle size in the range of 50-100  $\mu\text{m}$ . The surface of this complex is smoother than the surface of the other complexes.
- (7) The Sn(IV) complex particles have a cave-like-shaped morphology with a particle size of  $\sim 10 \mu\text{m}$ .
- (8) The Zn(II) complex has a crushed ice granular-shaped morphology with a particle size of 10  $\mu\text{m}$ . In addition, bright white particles were observed.
- (9) The peaks refer to essential elements, such as carbon, nitrogen, oxygen and subsidiary elements, that constitute the molecules of these complexes. These elements were clearly identifiable, and the results confirmed the proposed structures.

### 3.11 Pharmacology assessment

The pharmacological evaluation of HMDA and its CT complexes involved antibacterial and antifungal activity studies. The screenings were performed with a 100  $\mu\text{g/ml}$  concentration of the test CT complexes and an antibiotic disk. The diameter zones were measured to determine their effects on the growth of the tested microorganisms. The antibacterial activity of HMDA and its CT complexes was screened *in vitro* against two Gram-positive bacterial strains (i.e., *Staphylococcus aureus* (*S. aureus*) and *Bacillus subtilis*) and two Gram-negative bacterial strains (i.e., *Escherichia coli* (*E. coli*) and *Pseudomonas aeruginosa* (*P. aeruginosa*)). The activity was determined by measuring the inhibition zone diameter (mm) of the complexes against the microorganisms. Tetracycline was employed as the standard drug (positive control) for comparison of the bacterial results. The results from the agar disk diffusion tests are presented in Table 7 and statistically illustrated in Figure 11. The synthesized HMDA CT complexes were also examined for their antifungal properties against two fungal species including *Aspergillus flavus* and *Candida albicans*. Amphotericin B was employed as the standard drug (positive control) for comparison of the antifungal results. The screening data are reported in Table 7 and statistically represented in Figure 12. By comparing the biological activity of HMDA and its CT complexes, the following results were obtained:

- (1) The [(HMDA)(QL)] complex showed excellent antifungal activity against the growth of the tested fungal strains. The free HMDA exhibited no such activity, which makes this an interesting complex. This complex is comparable to Amphotericin B.
- (2) The [(HMDA)(QL)] and [(HMDA)(SnCl<sub>4</sub>)] complexes exhibited good inhibitory results against all of the Gram-positive and Gram-negative bacterial species.
- (3) The other HMDA complexes exhibited moderate antibacterial activity against all of the tested bacterial strains but had no inhibitory activity against either fungal strain.
- (4) The biological activity against the Gram-positive and Gram-negative bacteria followed the order: [(HMDA)(QL)] > [(HMDA)(SnCl<sub>4</sub>)] > [(HMDA)(ZnCl<sub>2</sub>)] > [HMDA]·2Br<sub>2</sub> > [HMDA-I]<sup>+</sup>I<sub>3</sub><sup>-</sup> > [(HMDA)(PA)<sub>2</sub>].

- (5) The antibacterial activity of the HMDA CT complexes is higher than that of the free HMDA.
- (6) The antibacterial activity of the HMDA and its complexes are lower than that of the tetracycline standard.
- (7) The Sn(IV) complex was found to be an efficient antibacterial agent, while the QL complex was found to be an efficient antibacterial and antifungal agent.

## References

- [1] I.M. Khan, A. Ahmad, S. Kumar, *J. Mol. Struct.* 1035 (2013) 38.
- [2] M. Shukla, N. Srivastava, S. Saha, *J. Mol. Struct.* 1021 (2012) 153.
- [3] M.S. Refat, H.A. Saad, A.M.A. Adam, *J. Mol. Struct.* 995 (2011) 116.
- [4] E.M. Nour, M.S. Refat, *J. Mol. Struct.* 994 (2011) 289.
- [5] M.S. Refat, A. Elfalaky, E. Elesh, *J. Mol. Struct.* 990 (2011) 217.
- [6] S.Y. AlQaradawi, A. Mostafa, H.S. Bazzi, *J. Mol. Struct.* 1011 (2012) 172.
- [7] R. Foster, *Organic Charge-Transfer Complexes*, Academic Press Inc., New York, 1969.
- [8] F. Gutmann, C. Johnson, H. Keyzer, J. Molnar, *Charge-Transfer Complexes in Biochemical Systems*, Marcel Dekker Inc., 1997.
- [9] I.M. Khan, A. Ahmad, M. Aatif, *J. Photochem. Photobiol. B: Biol.* 105 (2011) 6.
- [10] A.M.A. Adam, *Spectrochim. Acta A* 104 (2013) 1.
- [11] A.M.A. Adam, M.S. Refat, T. Sharshar, Z.K. Heiba, *Spectrochim. Acta A* 95 (2012) 458.
- [12] D.A. Skoog, *Principle of Instrumental Analysis*, third edn., Saunders College Publishing, New York, USA, 1985, Ch. 7.
- [13] H.A. Benesi, J.H. Hildebrand, *J. Am. Chem. Soc.* 71 (1949) 2703.
- [14] R. Abu-Eittah, F. Al-Sugeir, *Can. J. Chem.* 54 (1976) 3705.
- [15] A.W. Bauer, W.M. Kirby, C. Sherris, M. Turck, *Am. J. Clin. Pathol.* 45 (1966) 493.
- [16] M.A. Pfaller, L. Burmeister, M.A. Bartlett, M.G. Rinaldi, *J. Clin. Microbiol.* 26 (1988) 1437.
- [17] D.J. Beecher, A.C. Wong, *Appl. and Environ. Microbiol.* 60 (1994) 1646.
- [18] National Committee for Clinical Laboratory Standards. *Methods for Antimicrobial Susceptibility Testing of Anaerobic Bacteria: Approved Standard M11-A3*. NCCLS, Wayne, PA, USA (1993).
- [19] National Committee for Clinical Laboratory Standards. *Reference Method for Broth Dilution Antifungal Susceptibility Testing of Conidium-Forming Filamentous Fungi: Proposed Standard M38-A*. NCCLS, Wayne, PA, USA (2002).
- [20] National Committee for Clinical Laboratory Standards. *Method for Antifungal Disk Diffusion Susceptibility Testing of Yeast: Proposed Guideline M44-P*. NCCLS, Wayne, PA, USA (2003).
- [21] M. Pandeewaran, K.P. Elango, *Spectrochim. Acta A* 72 (2009) 789.
- [22] G. Briegleb, *Z. Angew. Chem.* 76 (1964) 326.
- [23] H. Tsubomura, R.P. Lang, *J. Am. Chem. Soc.* 83 (1961) 2085.
- [24] R. Rathone, S.V. Lindeman, J.K. Kochi, *J. Am. Chem. Soc.* 119 (1997) 9393.
- [25] A.N. Martin, J. Swarbrick, A. Cammarata, *Physical Pharmacy*, third edn., Lee and Febiger, Philadelphia, PA, 1969, p. 344.
- [26] M. Pandeewaran, K.P. Elango, *J. Indian Chem. Soc.* 85 (2008) 399.
- [27] K.M. Al-Ahmary, M.M. Habeeb, E.A. Al-Solmy, *J. Mol. Liq.* 162 (2011) 129.
- [28] M.S. Refat, H.A. Saad, A.A. Adam, *J. Mol. Struct.* 995 (2011) 116.

- [29] A.S. Gaballa, S.M. Teleb, E. Nour, *J. Mol. Struct.* 1024 (2012) 32.
- [30] A.A. Adam, *J. Mol. Struct.* 1030 (2012) 26.
- [31] K. Nakamoto, *Infrared and Raman Spectra of Inorganic and Coordination Compounds, Parts A and B*, John Wiley and Sons, New York, 1997.
- [32] M. Pandeewaran, K.P. Elango, *Spectrochim. Acta A* 72 (2009) 789.
- [33] A.G. Maki, R. Forneris, *Spectrochim. Acta A* 23 (1967) 867.
- [34] W. Kiefer, H.J. Bernstein, *Chem. Phys. Lett.* 16 (1972) 5.
- [35] L. Andrews, E.S. Prochaska, A. Loewenschuss, *Inorg. Chem.* 19 (1980) 463.
- [36] K. Kaya, N. Mikami, Y. Udagawa, M. Ito, *Chem. Phys. Lett.* 16 (1972) 151.
- [37] R.D. Kross, V.A. Fassel, *J. Am. Chem. Soc.* 79 (1957) 38.
- [38] N. Singh, A. Ahmad, *J. Mol. Struct.* 977 (2010) 197.
- [39] A.W. Coats, J.P. Redfern, *Nature (London)* 201 (1964) 68.
- [40] H.H. Horowitz, G. Metzger, *Anal. Chem.* 35 (1963) 1464.
- [41] S.J.S. Qazi, A.R. Rennie, J.K. Cockcroft, M. Vickers, *J. Colloid Interface Sci.* 338 (2009) 105.

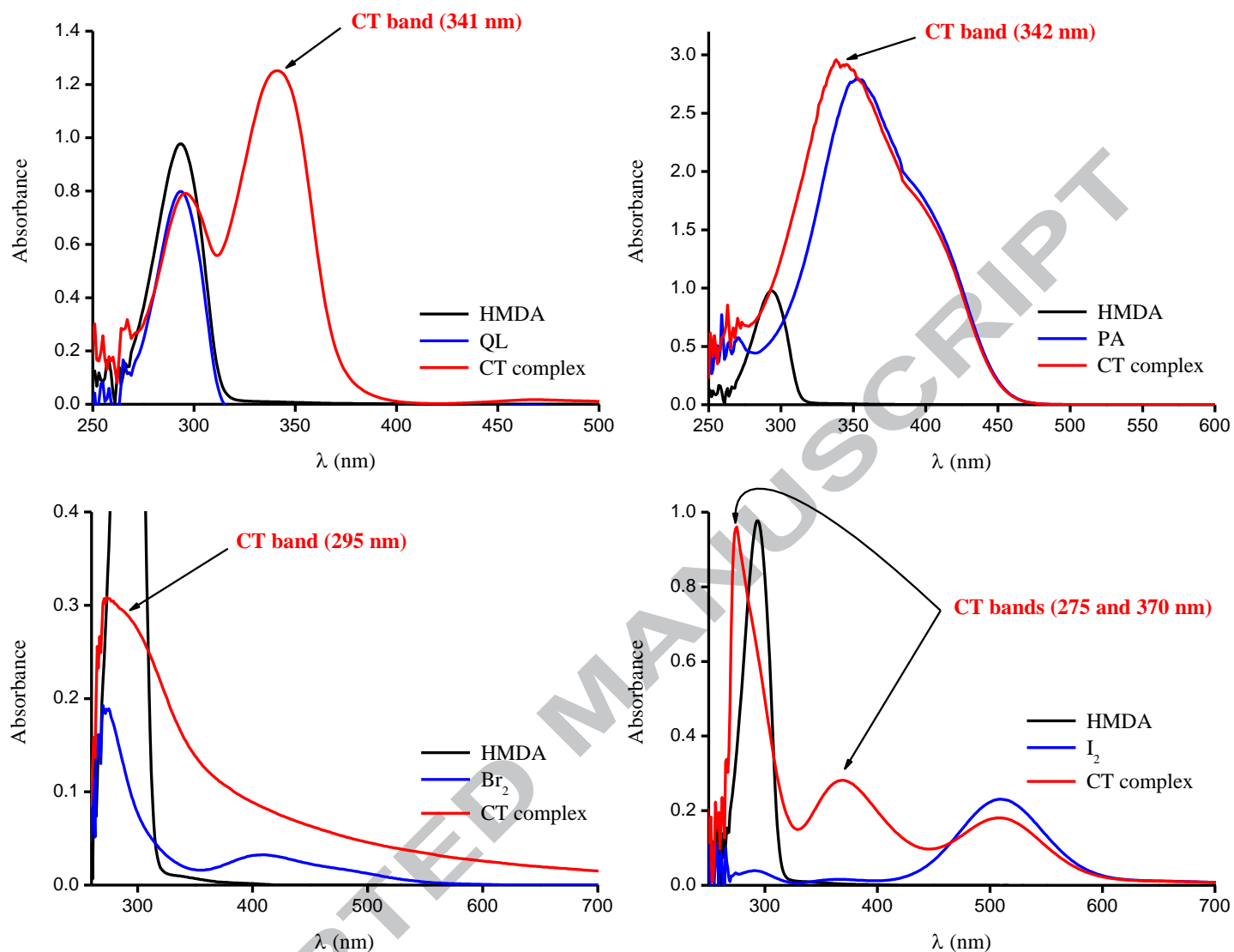


**Figure 1.** Electronic spectra of [(HMDA)(QL)], [(HMDA)(PA)<sub>2</sub>], [HMDA]·2Br<sub>2</sub> and [HMDA-I]<sup>+</sup>I<sub>3</sub><sup>-</sup> charge-transfer complexes in methanol solvent.

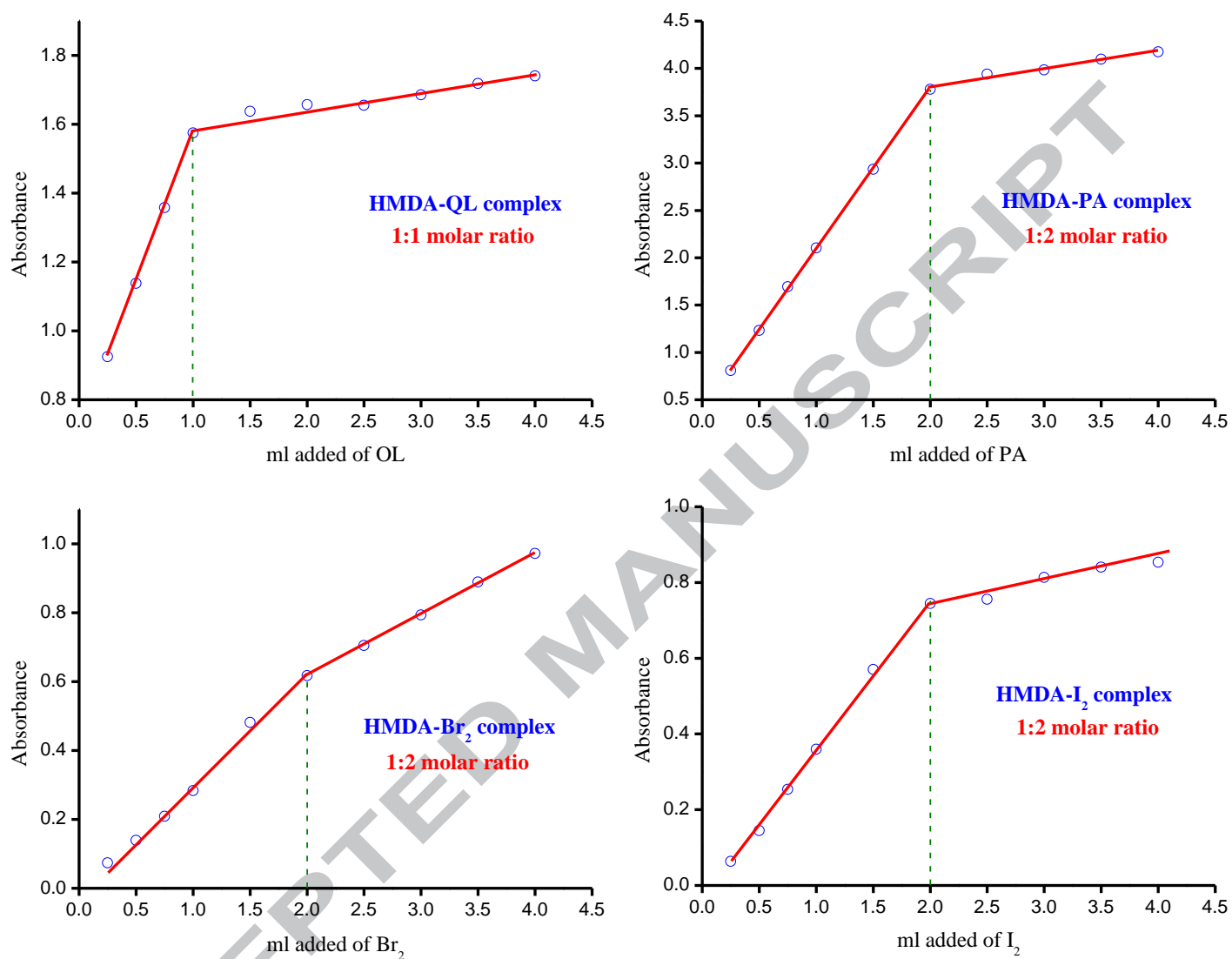


**Figure 2.** Spectrophotometric titration curves of [(HMDA)(QL)], [(HMDA)(PA)<sub>2</sub>], [HMDA]·2Br<sub>2</sub> and [HMDA-I]<sup>+</sup>I<sub>3</sub><sup>-</sup> charge-transfer complexes in methanol solvent.

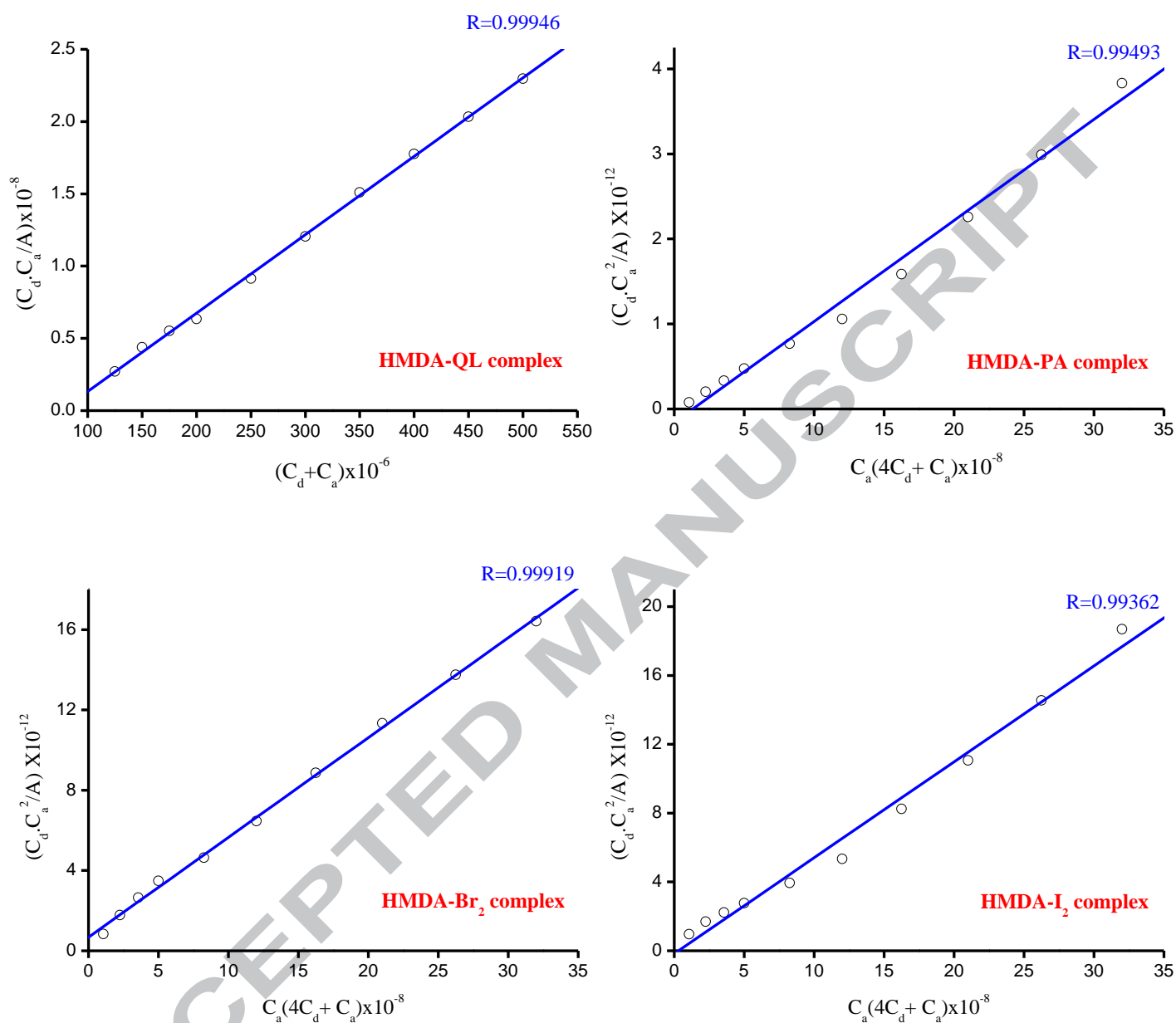


**Figure 3.** The 1:1 and 1:2 Benesi-Hildebrand plot of [(HMDA)(QL)], [(HMDA)(PA)<sub>2</sub>], [HMDA]·2Br<sub>2</sub> and [HMDA-I]<sup>+</sup>I<sub>3</sub><sup>-</sup> charge-transfer complexes.

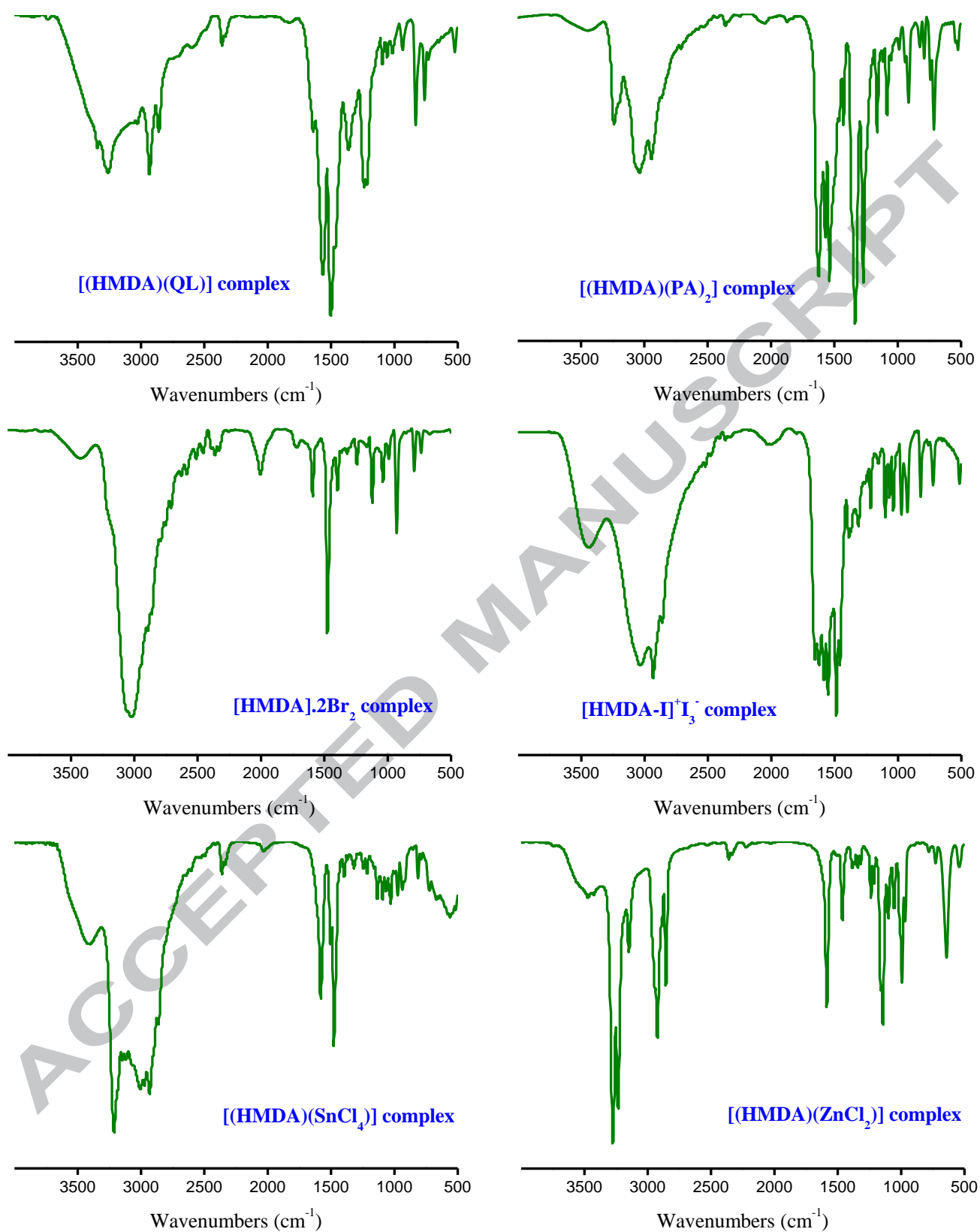


**Figure 4.** Infrared spectra of HMDA charge-transfer complexes.

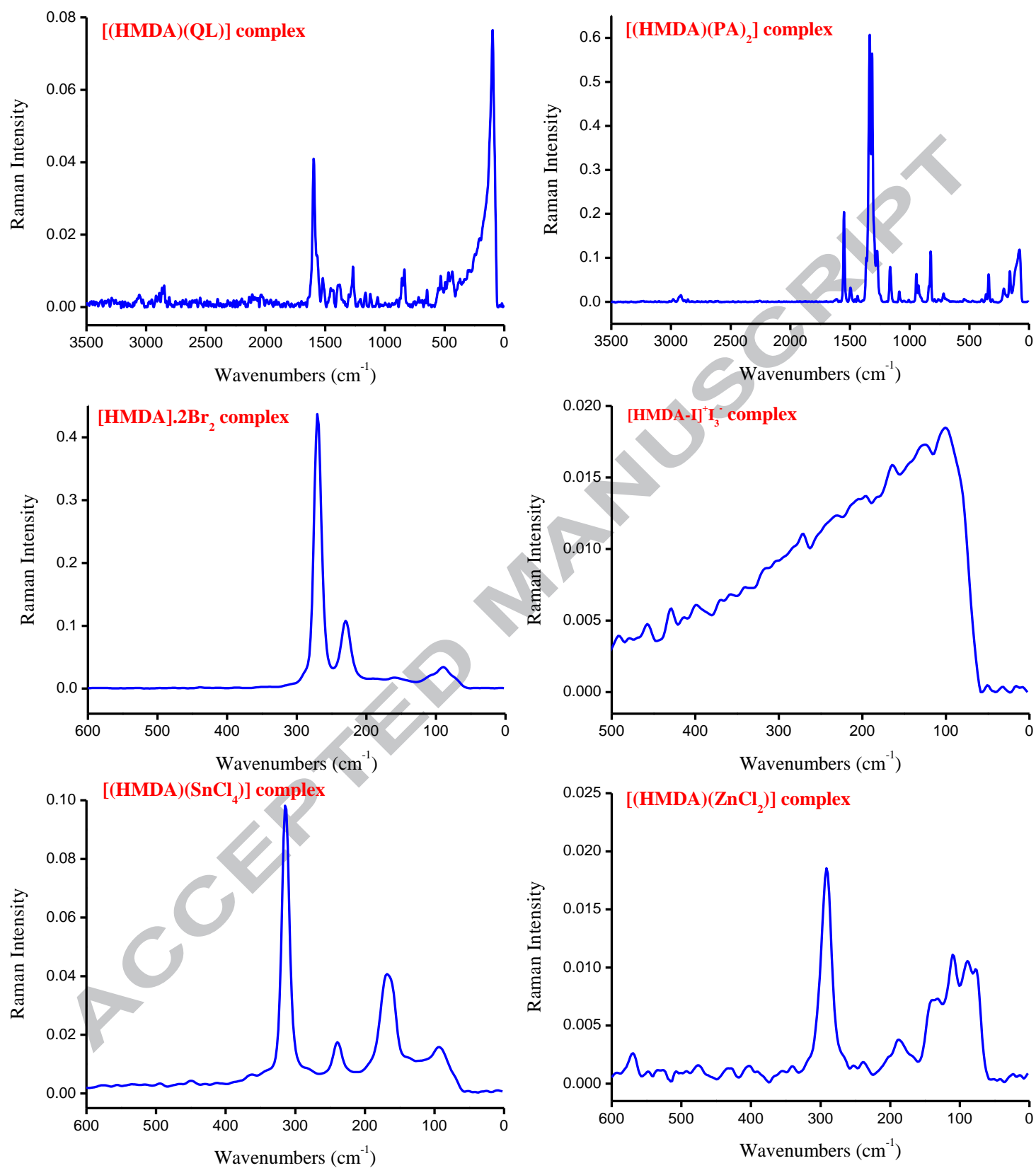


**Figure 5.** Laser Raman spectra of HMDA charge-transfer complexes.

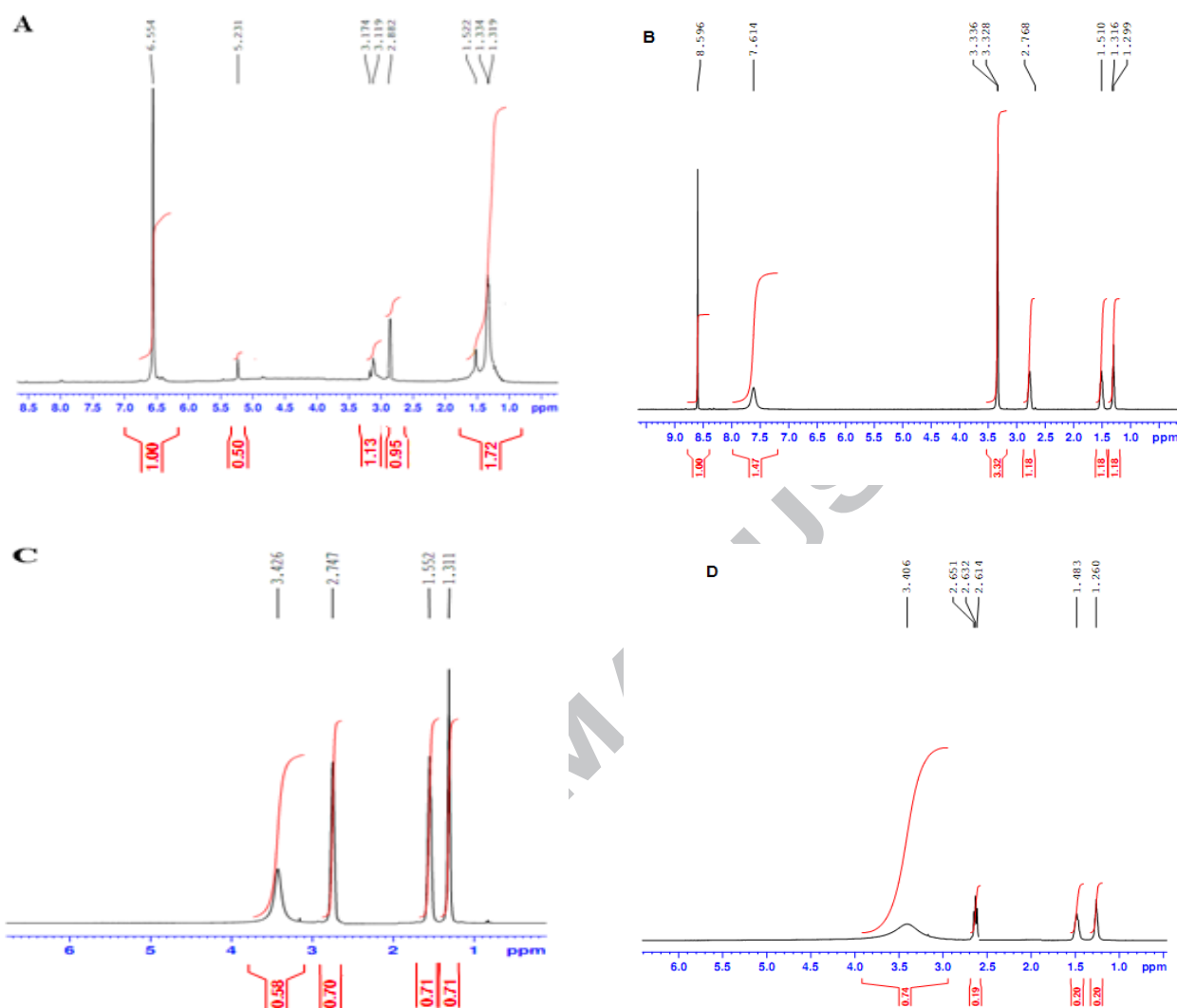


**Figure 6.**  $^1\text{H}$  NMR spectrum of (A)  $[(\text{HMDA})(\text{QL})]$ , (B)  $[(\text{HMDA})(\text{PA})_2]$ , (C)  $[(\text{HMDA})(\text{SnCl}_4)]$  and  $[(\text{HMDA})(\text{ZnCl}_2)]$  CT complexes.

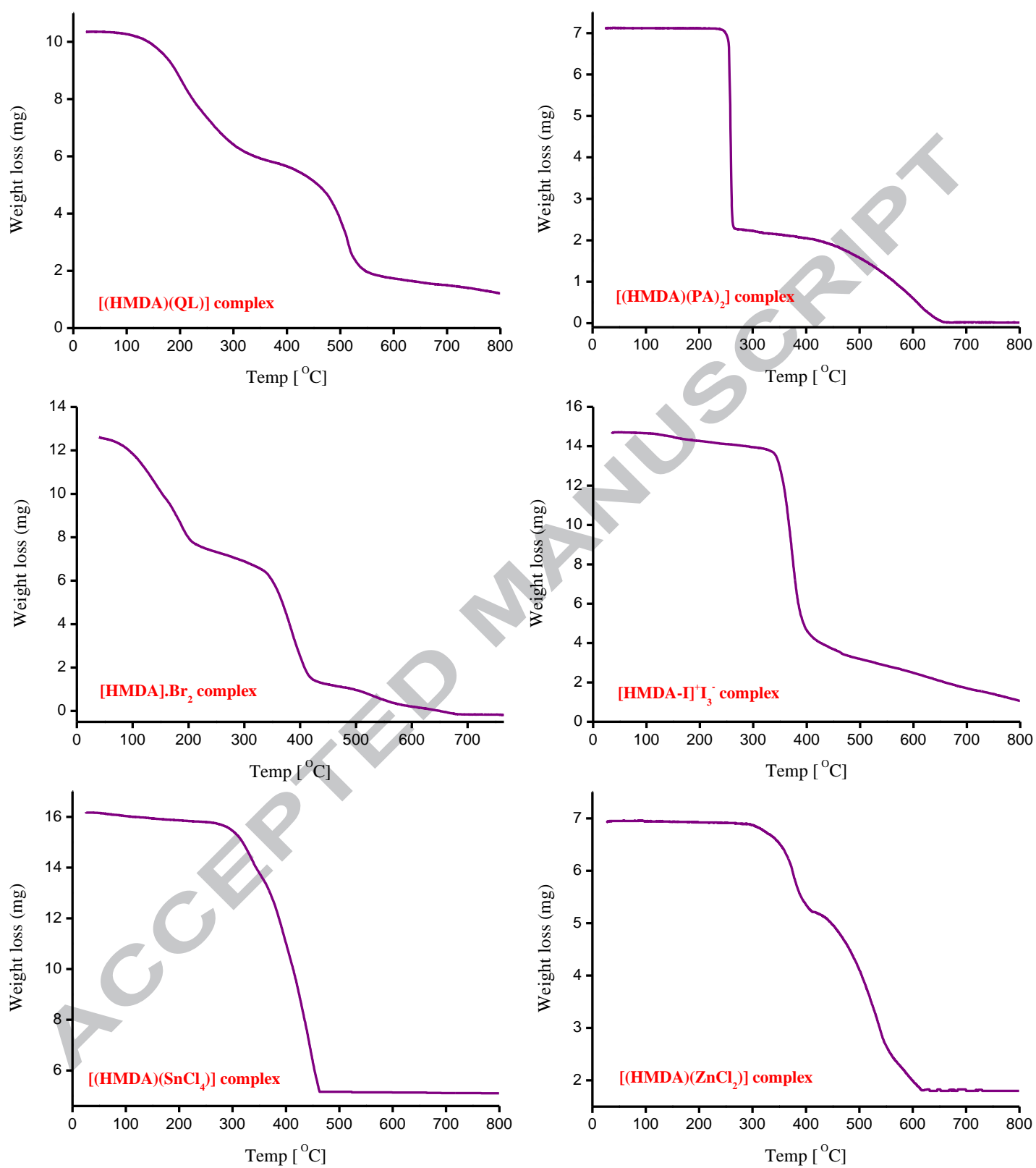


**Figure 7.** TG curves of HMDA charge-transfer complexes.

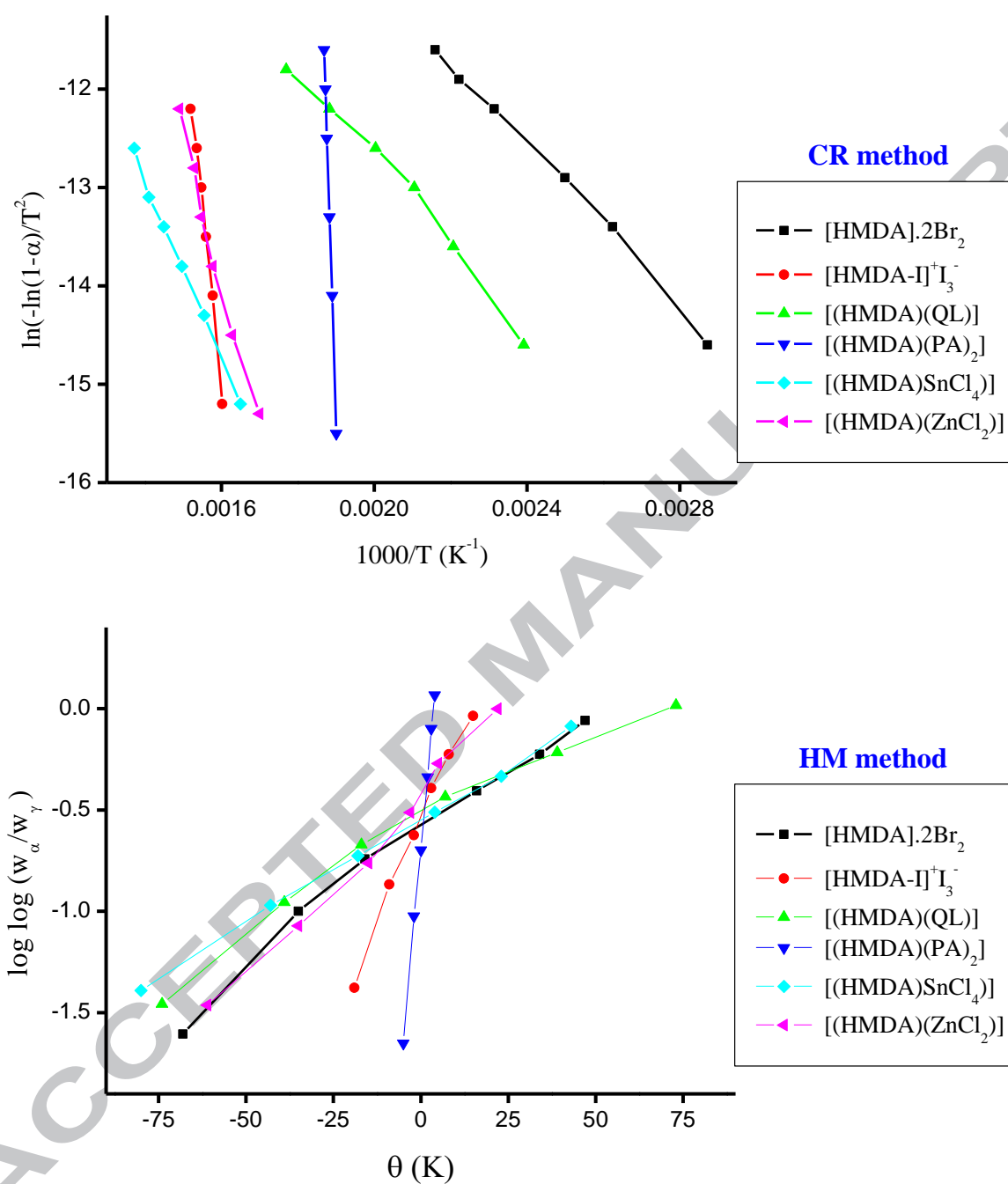


**Figure 8.** Kinetic curves for HMDA charge-transfer complexes (CR; Coats-Redfern equation, HM; Horowitz-Metzger (HM) equation).

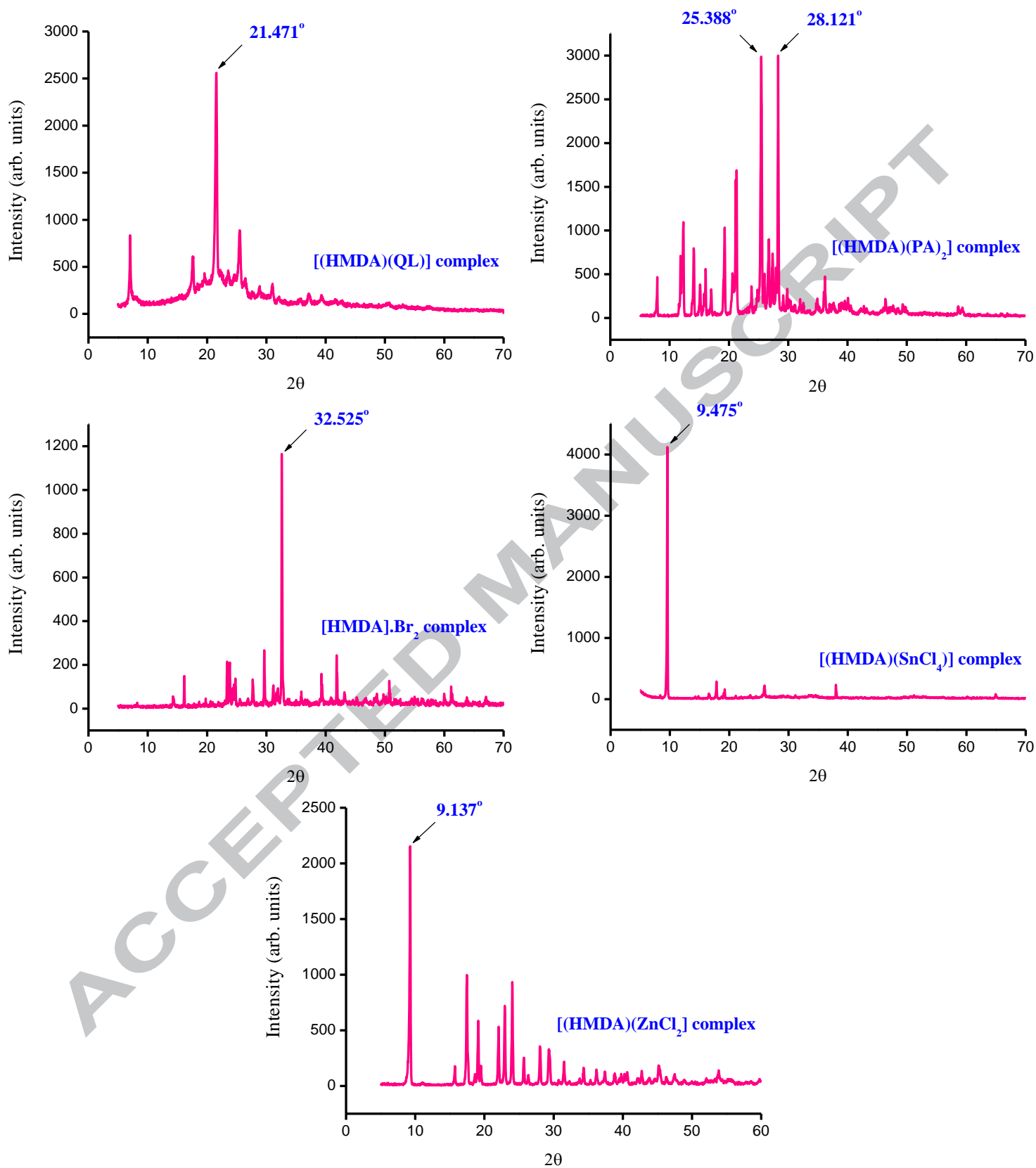


**Figure 9.** XRD spectra of HMDA CT complexes.

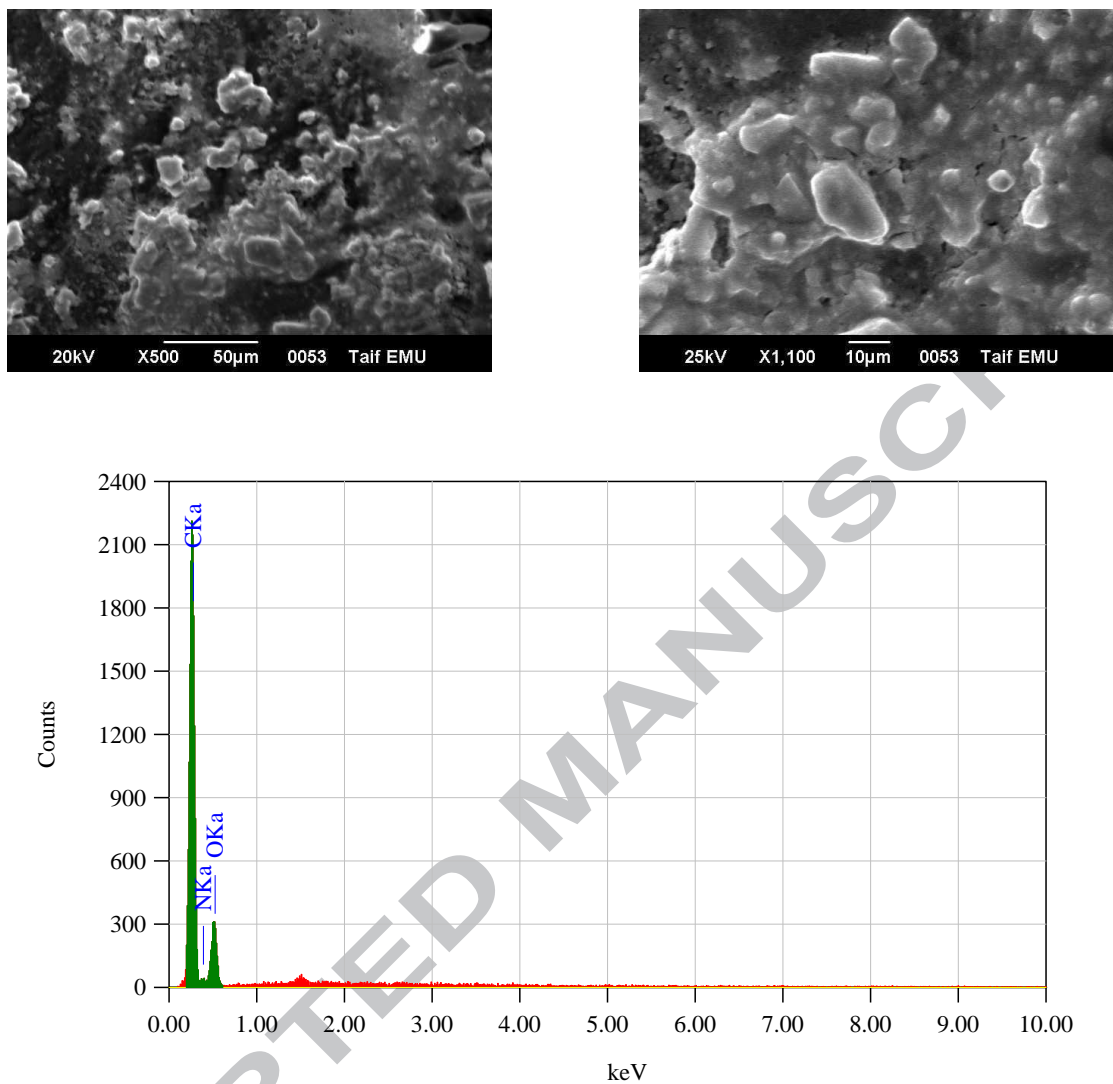


**Figure 10A.** SEM images and EDX spectrum of [(HMDA)(QL)] complex.

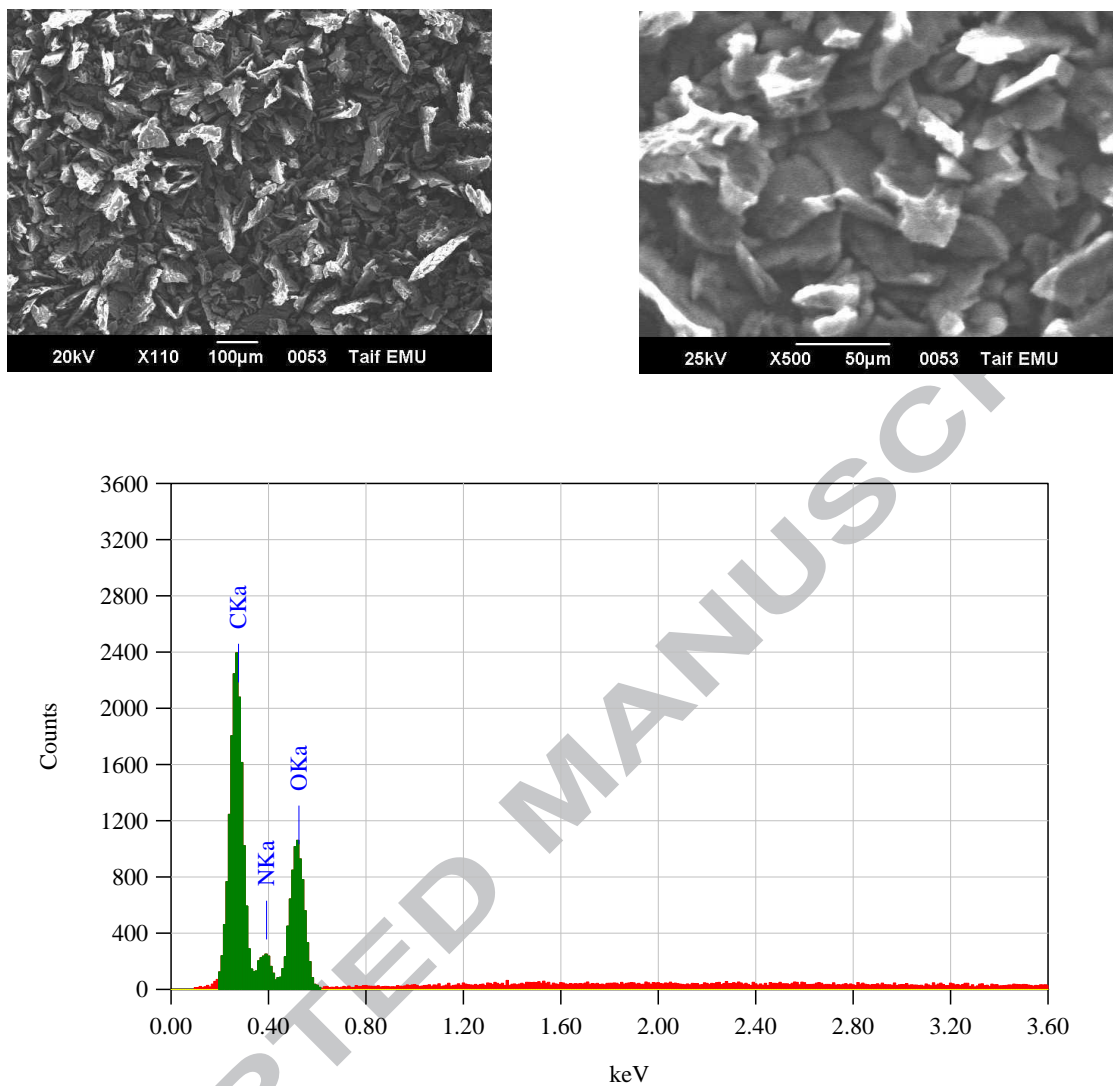


**Figure 10B.** SEM images and EDX spectrum of [(HMDA)(PA)<sub>2</sub>] complex.

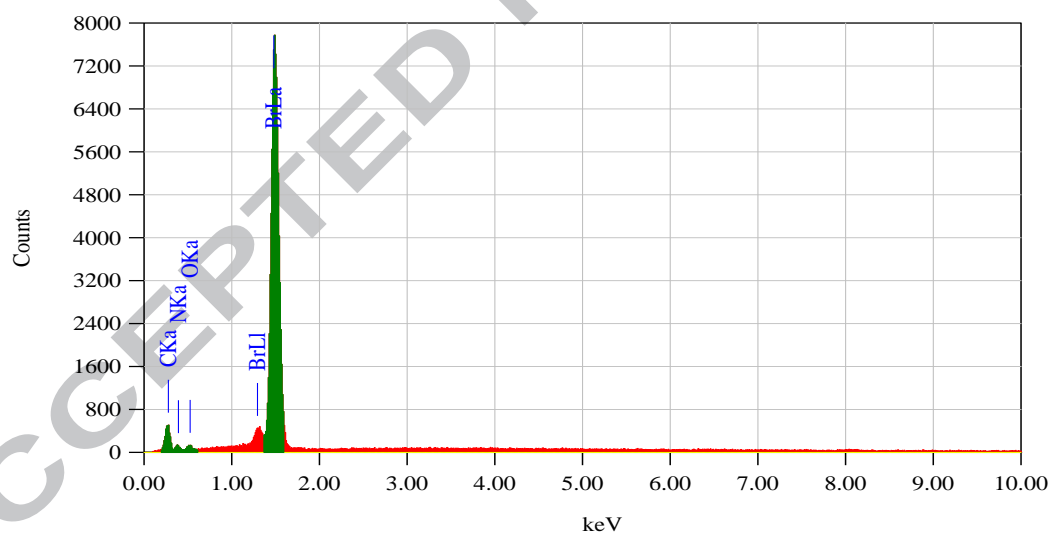
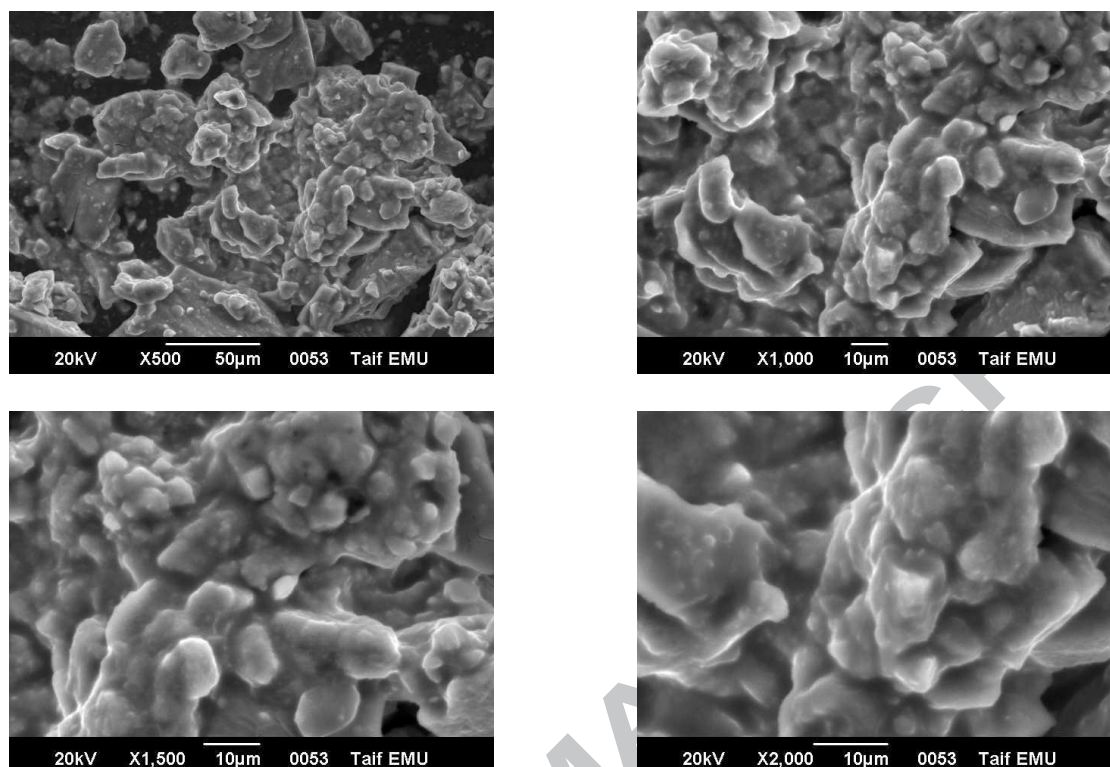


**Figure 10C.** SEM images and EDX spectrum of [HMDA]·Br<sub>2</sub> complex.

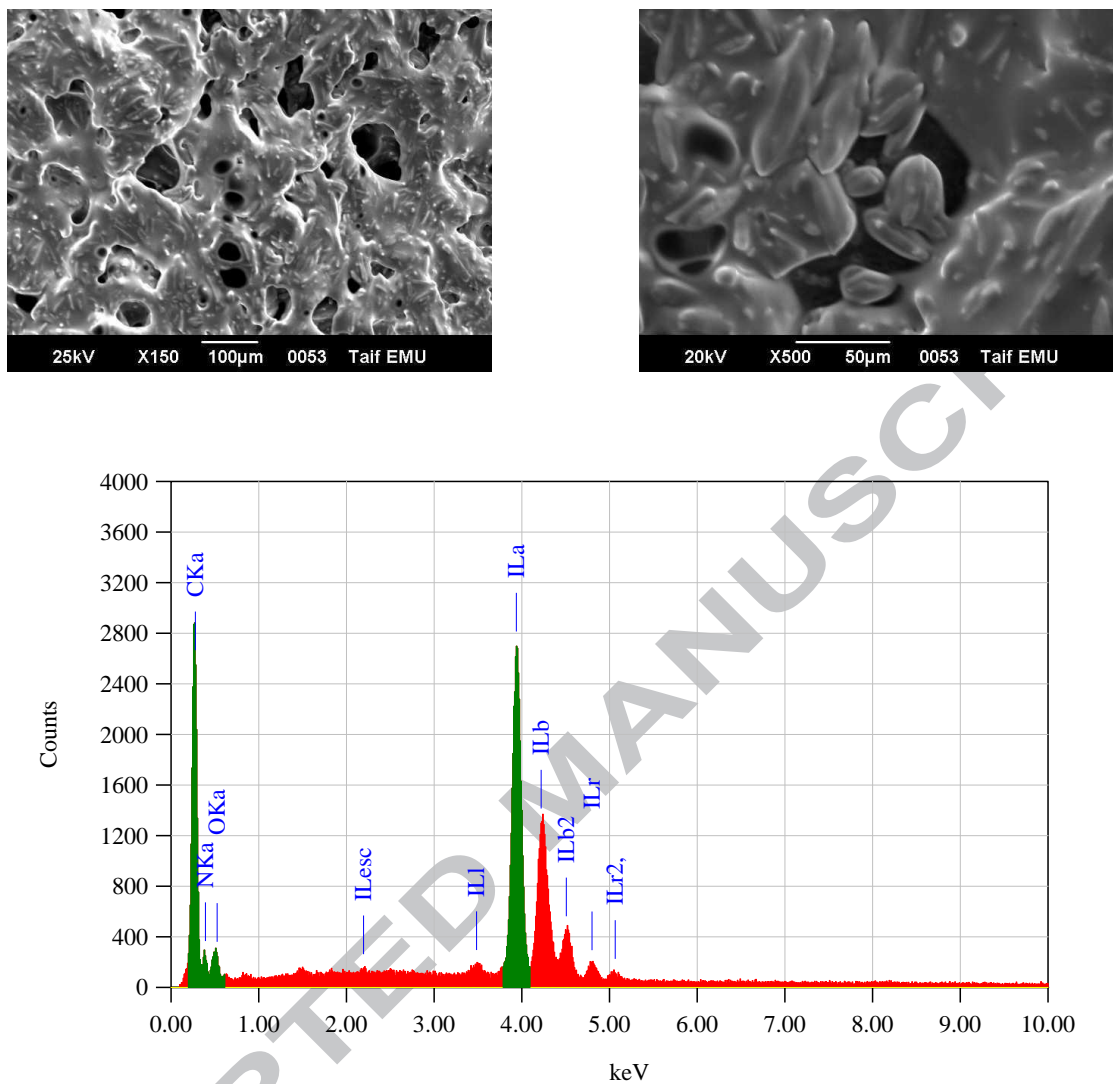


**Figure 10D.** SEM images and EDX spectrum of  $[\text{HMDA-I}]^+\text{I}_3^-$  complex.

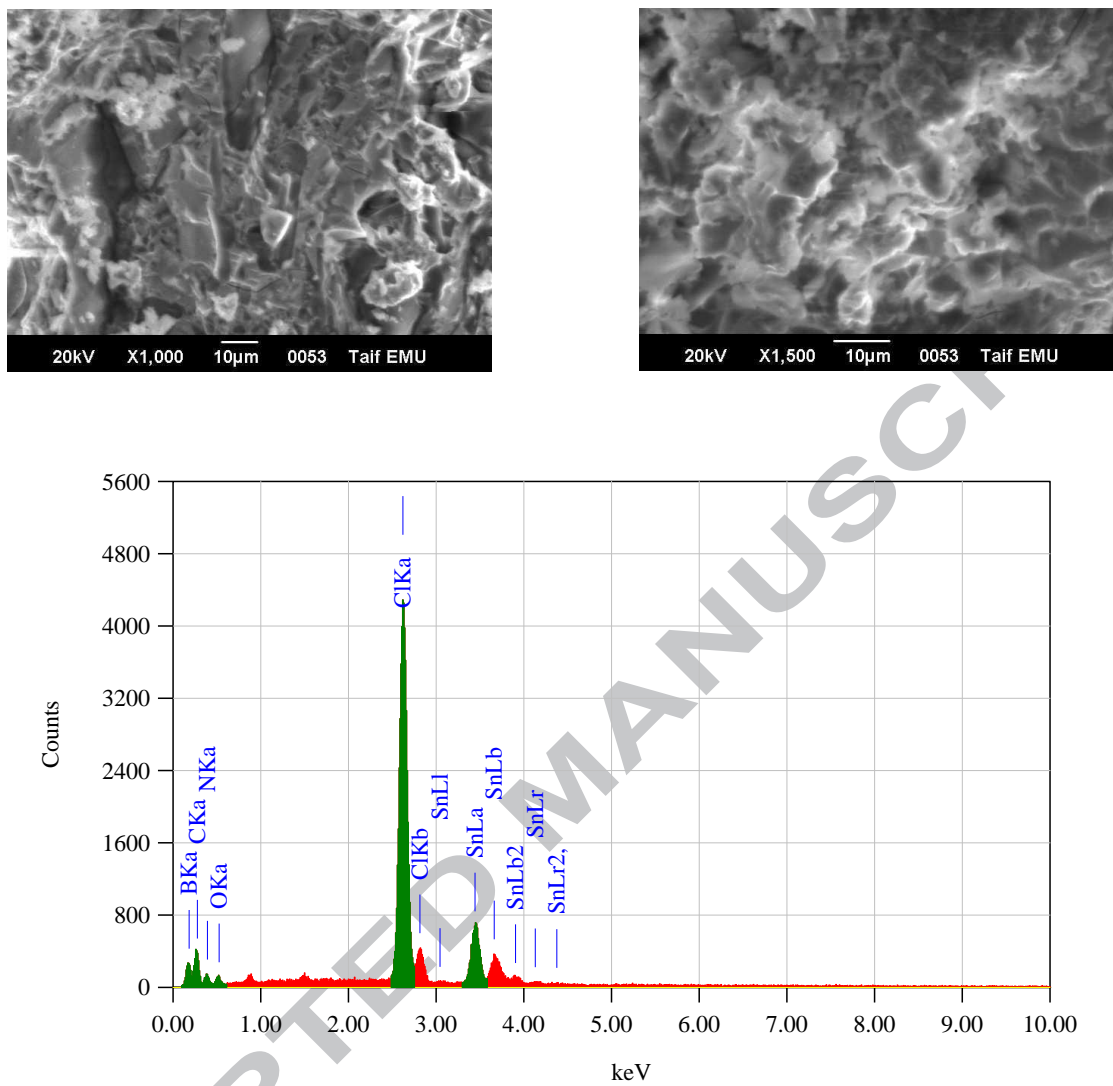


**Figure 10E.** SEM images and EDX spectrum of [(HMDA)(SnCl<sub>4</sub>)] complex.

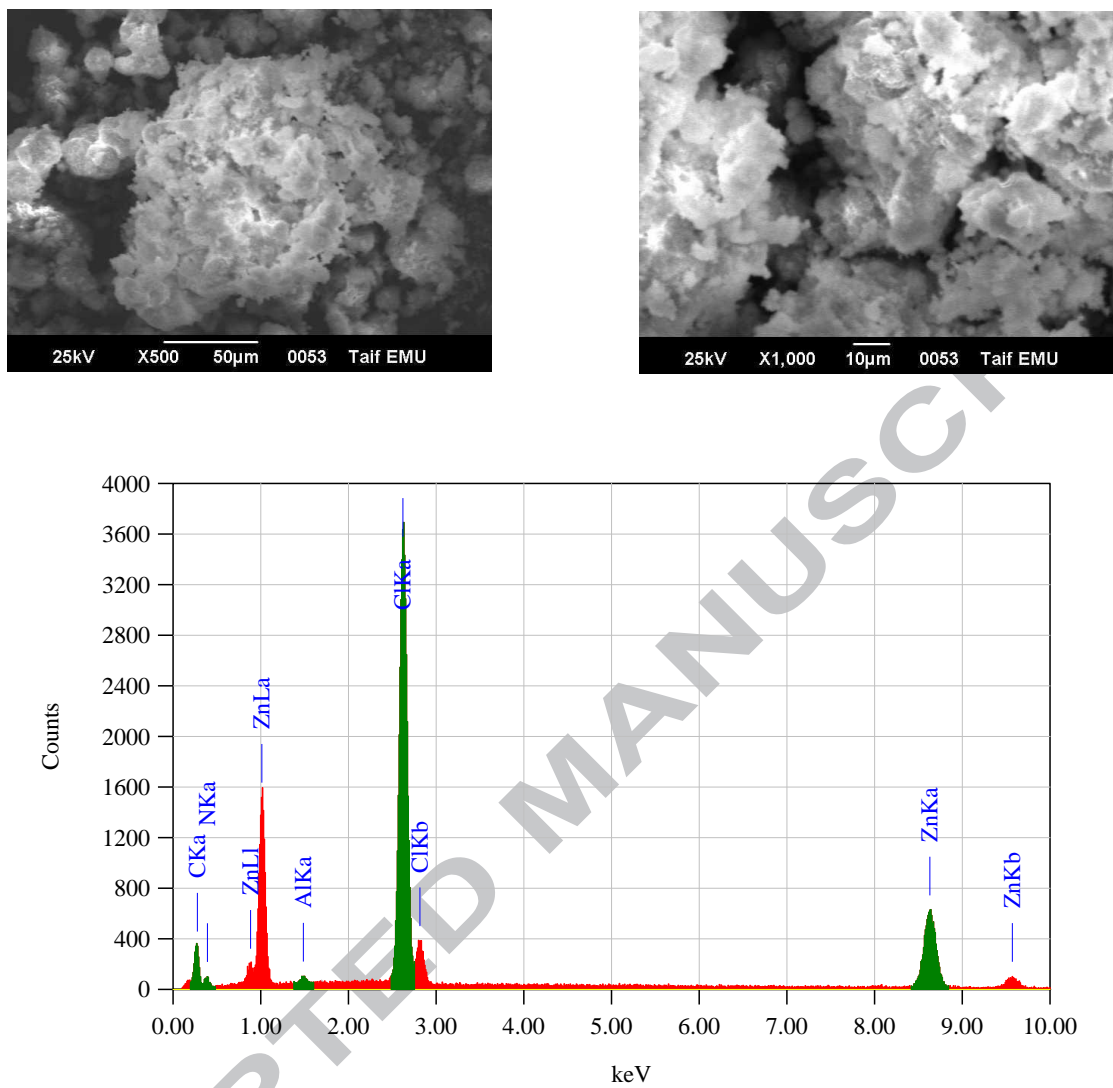


**Figure 10F.** SEM images and EDX spectrum of [(HMDA)(ZnCl<sub>2</sub>)] complex.

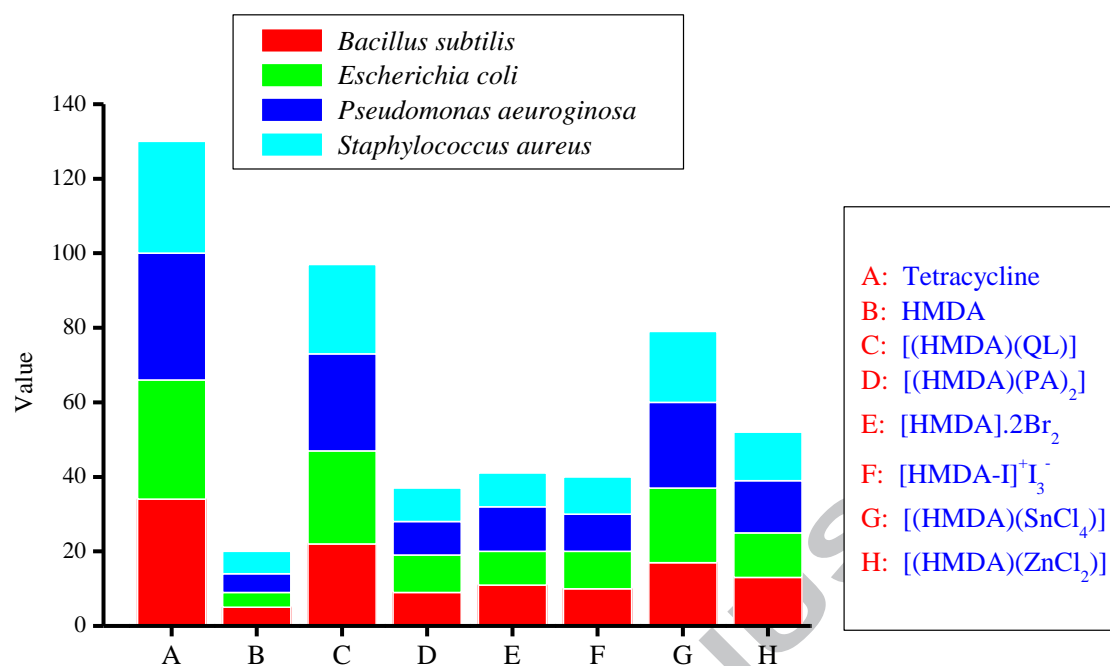


**Figure 11.** Statistical representation for antibacterial activity of HMDA CT complexes.

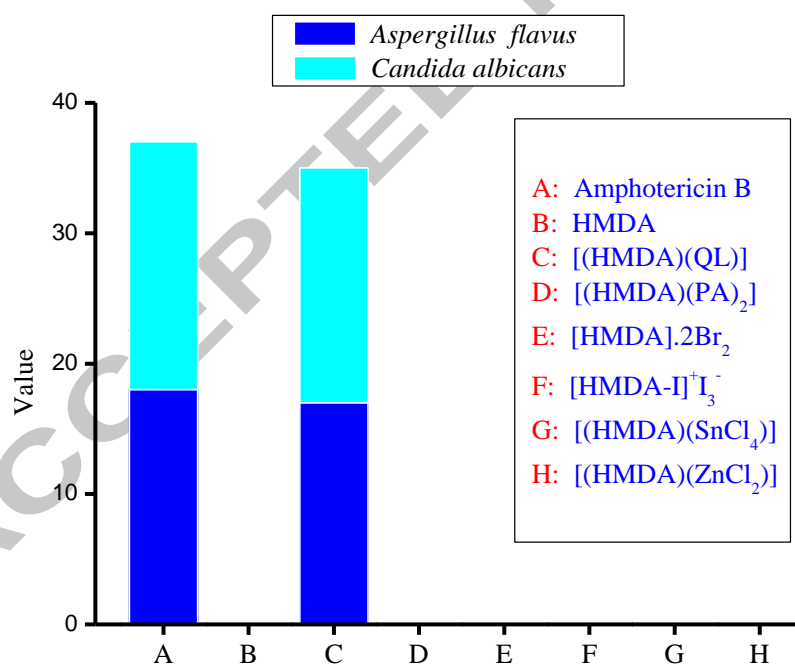


**Figure 12.** Statistical representation for antifungal activity of HMDA CT complexes.

**Table 1**

Analytical and physical data of the HMDA CT complexes.

Complex	Molecular formula	Mwt. g/mol	Elemental analyses						Molar ratio	Color
			C%		H%		N%			
			Found	Calc.	Found	Calc.	Found	Calc.		
[(HMDA)(QL)]	C <sub>12</sub> H <sub>22</sub> N <sub>2</sub> O <sub>2</sub>	226.31	63.27	63.63	9.67	9.72	12.25	12.37	1:1	Pale brown
[(HMDA)(PA) <sub>2</sub> ]	C <sub>18</sub> H <sub>22</sub> N <sub>8</sub> O <sub>14</sub>	574.40	37.76	37.60	3.99	3.83	19.60	19.50	1:2	Orange
[HMDA]·2Br <sub>2</sub>	C <sub>6</sub> H <sub>16</sub> N <sub>2</sub> Br <sub>4</sub>	435.80	16.50	16.52	3.47	3.67	6.46	6.42	1:2	Orange yellow
[HMDA-I] <sup>+</sup> I <sub>3</sub> <sup>-</sup>	C <sub>6</sub> H <sub>16</sub> N <sub>2</sub> I <sub>4</sub>	623.56	11.72	11.55	2.41	2.57	4.60	4.49	1:2	Reddish brown
[(HMDA)(SnCl <sub>4</sub> )]	C <sub>6</sub> H <sub>16</sub> N <sub>2</sub> SnCl <sub>4</sub>	376.70	19.27	19.11	4.22	4.25	7.38	7.43	1:1	White
[(HMDA)(ZnCl <sub>2</sub> )]	C <sub>6</sub> H <sub>16</sub> N <sub>2</sub> ZnCl <sub>2</sub>	252.52	28.47	28.51	6.30	6.34	11.14	11.09	1:1	White

**Table 2**

Spectroscopic and physical data of the HMDA CT complexes (25 °C).

Complex	$\lambda_{max}$ (nm)	$K$ (Lmol <sup>-1</sup> )	$\epsilon_{max}$ (Lmol <sup>-1</sup> cm <sup>-1</sup> )	$E_{CT}$ (eV)	$f$	$\mu$	$\Delta G^\circ$ (kJ mol <sup>-1</sup> )
[(HMDA)(QL)]	341	$1.32 \times 10^4$	$1.84 \times 10^4$	3.65	19.88	37.96	-34,926
[(HMDA)(PA) <sub>2</sub> ]	342	$7.53 \times 10^7$	$8.42 \times 10^4$	3.64	36.37	51.41	-44,943
[HMDA]·2Br <sub>2</sub>	275	$7.36 \times 10^7$	$2.01 \times 10^4$	4.22	24.81	39.44	-44,887
[HMDA-I] <sup>+</sup> I <sub>3</sub> <sup>-</sup>	370	$3.35 \times 10^7$	$1.79 \times 10^4$	3.36	25.83	45.07	-48,643

**Table 3**  
Infrared frequencies<sup>(a)</sup> (cm<sup>-1</sup>) and tentative assignments for HMDA CT complexes.

HMDA	[(HMDA)(QL)]	[(HMDA)(PA) <sub>2</sub> ]	[HMDA]·2Br <sub>2</sub>	[HMDA-I] <sup>+ -</sup> I <sub>3</sub> <sup>-</sup>	[(HMDA)(SnCl <sub>4</sub> )]	[(HMDA)(ZnCl <sub>2</sub> )]	Assignments <sup>(b)</sup>
3339	3349	3461	3433	3451	3411	3472	v(N-H)
-	3267	3240	-	-	-	-	v(OH···N), hydrogen bonding
2934, 2856	3030, 2948, 2866	3047, 2956	3029, 2800	3038, 2945, 2877	3015	3162, 2926 2862	v <sub>s</sub> (C-H) + v <sub>as</sub> (C-H); CH <sub>2</sub>
1660	-	-	1602	1650, 1555	-	-	δ <sub>def</sub> (N-H)
-	-	1638	-	-	-	-	v <sub>as</sub> (NO <sub>2</sub> ); PA complex
-	1576, 1503	1575, 1538	-	-	-	-	v(C=C)
1476, 1455	-	1438	1485	1491	1593, 1483	1598, 1470	δ(C-H) deformation
1395, 1360	1364	1338	1400	1388	1397, 1325	1387	
1284, 1237	1236	1274	1255, 1127	1306, 1224	1260, 1224	1238	v <sub>as</sub> (C-N)
1061, 1014	1095, 1058, 1022	1166, 1093	1051	1096, 1041	1151, 1105, 1023	1145, 1099, 1054	v <sub>s</sub> (C-N)
970, 878	940, 840	920, 829	931	969, 923	978, 942	999	δ <sub>rock</sub> , NH
823, 733	776	802, 720	805, 736	823, 723	823, 732	-	δ(CH) in-plane bending
611	524	526	-	522	669	644	δ(C-N) out-of-plane bending
-	-	460	-	-	-	-	δ(ONO); PA complex
-	-	-	-	-	538	544	v(M-N)

(a): s, strong; w, weak; m, medium; sh, shoulder; v, very; vs, very strong; br, broad.

(b): v, stretching; v<sub>s</sub>, symmetrical stretching; v<sub>as</sub>, asymmetrical stretching; δ, bending.

**Table 4**

Thermal decomposition data for the HMDA CT complexes.

Complex	Decomposition	TG range (°C)	Lost Species	% Weight loss	
				Found	Calculated
[(HMDA)(QL)]	First step	25-230	C <sub>2</sub> H <sub>8</sub> N <sub>2</sub>	26.29	26.51
	Second step	230-514	C <sub>5</sub> H <sub>4</sub> O <sub>2</sub>	42.81	42.42
	Third step	514-800	C <sub>3</sub> H <sub>10</sub>	19.98	20.33
	Total loss			89.08	89.26
	Residue		2C	10.92	10.60
[(HMDA)(PA) <sub>2</sub> ]	First step	25-370	C <sub>7</sub> H <sub>12</sub> N <sub>8</sub> O <sub>14</sub>	70.49	69.71
	Second step	370-800	C <sub>11</sub> H <sub>10</sub>	29.51	30.29
	Total loss			100	100
	Residue		-	-	-
[HMDA]·2Br <sub>2</sub>	First step	25-265	Br <sub>2</sub> + 2CH <sub>4</sub>	43.86	44.01
	Second step	265-468	Br <sub>2</sub> + CH <sub>4</sub> + N <sub>2</sub>	46.80	46.77
	Third step	468-800	CH <sub>4</sub> + 2CO <sub>2</sub>	9.34	9.18
	Total loss			100	99.96
	Residue		-	-	-
[HMDA-I] <sup>+</sup> I <sub>3</sub> <sup>-</sup>	First step	25-460	2I <sub>2</sub>	81.40	81.31
	Second step	460-800	4CH <sub>4</sub> + N <sub>2</sub>	14.75	14.64
	Total loss			96.15	95.95
	Residue		2C	3.85	4.01
[(HMDA)(SnCl <sub>4</sub> )]	First step	25-800	C <sub>6</sub> H <sub>16</sub> N <sub>2</sub> Cl <sub>4</sub>	68.52	68.50
	Total loss			68.52	68.50
	Residue		Sn metal	31.48	31.46
[(HMDA)(ZnCl <sub>2</sub> )]	First step	25-367	C <sub>2</sub> H <sub>8</sub> N <sub>2</sub>	23.71	23.76
	Second step	367-546	C <sub>4</sub> H <sub>8</sub> Cl	36.40	36.23
	Third step	546-800	½Cl <sub>2</sub>	14.09	14.06
	Total loss			74.20	74.05
	Residue		Zn metal	25.80	25.89

**Table 5**

Kinetic parameters determined using the Coats-Redfern (CR) and Horowitz-Metzger (HM) methods.

Complex	Method	Parameters <sup>a</sup>					<i>r</i>
		<i>E</i> <sup>*</sup>	<i>A</i>	$\Delta S^*$	$\Delta H^*$	$\Delta G^*$	
[(HMDA)(QL)]	CR	$3.73 \times 10^4$	$2.67 \times 10^1$	$-2.22 \times 10^2$	$3.32 \times 10^4$	$1.42 \times 10^5$	0.99201
	HM	$4.56 \times 10^4$	$3.95 \times 10^2$	$-1.99 \times 10^2$	$4.15 \times 10^4$	$1.40 \times 10^5$	0.98362
[(HMDA)(PA) <sub>2</sub> ]	CR	$1.01 \times 10^6$	$4.35 \times 10^{97}$	$1.62 \times 10^3$	$1.00 \times 10^6$	$1.41 \times 10^5$	0.99961
	HM	$1.02 \times 10^6$	$3.17 \times 10^{99}$	$1.66 \times 10^3$	$1.02 \times 10^6$	$1.38 \times 10^5$	0.99914
[HMDA]·2Br <sub>2</sub>	CR	$3.42 \times 10^4$	$6.88 \times 10^1$	$-2.13 \times 10^2$	$3.07 \times 10^4$	$1.19 \times 10^5$	0.99787
	HM	$4.27 \times 10^4$	$1.70 \times 10^3$	$-1.86 \times 10^2$	$3.93 \times 10^4$	$1.17 \times 10^5$	0.99142
[HMDA-I] <sup>+</sup> I <sub>3</sub> <sup>-</sup>	CR	$3.05 \times 10^5$	$8.84 \times 10^{22}$	$1.88 \times 10^2$	$3.00 \times 10^5$	$1.79 \times 10^5$	0.99588
	HM	$3.13 \times 10^5$	$6.58 \times 10^{23}$	$2.05 \times 10^2$	$3.08 \times 10^5$	$1.77 \times 10^5$	0.99388
[(HMDA)(SnCl <sub>4</sub> )]	CR	$7.53 \times 10^4$	$1.78 \times 10^3$	$-1.90 \times 10^2$	$6.96 \times 10^4$	$2.00 \times 10^5$	0.99847
	HM	$9.34 \times 10^4$	$7.68 \times 10^3$	$-1.58 \times 10^2$	$8.77 \times 10^4$	$1.96 \times 10^5$	0.99926
[(HMDA)(ZnCl <sub>2</sub> )]	CR	$1.24 \times 10^5$	$6.71 \times 10^7$	$-1.02 \times 10^2$	$1.18 \times 10^5$	$1.84 \times 10^5$	0.99141
	HM	$1.44 \times 10^5$	$4.18 \times 10^9$	$-6.72 \times 10^1$	$1.39 \times 10^5$	$1.39 \times 10^5$	0.99504

<sup>a</sup> Units of parameters: *E* in kJ mol<sup>-1</sup>, *A* in s<sup>-1</sup>,  $\Delta S$  in J mol<sup>-1</sup>K<sup>-1</sup>,  $\Delta H$  and  $\Delta G$  in kJ mol<sup>-1</sup>.

**Table 6**

XRD spectral data of HMDA CT complexes.

Complex	2 $\theta$ ( $^{\circ}$ )	d value ( $\text{\AA}$ )	$\beta$ ; FWHM	Particle size (nm)
[(HMDA)(QL)]	21.471	4.135	0.3	4.913
[(HMDA)(PA) <sub>2</sub> ]	28.121	3.171	0.2	7.464
[HMDA]·2Br <sub>2</sub>	32.525	2.751	0.15	10.06
[(HMDA)(SnCl <sub>4</sub> )]	9.475	9.327	0.125	11.62
[(HMDA)(ZnCl <sub>2</sub> )]	9.137	9.671	0.2	7.263

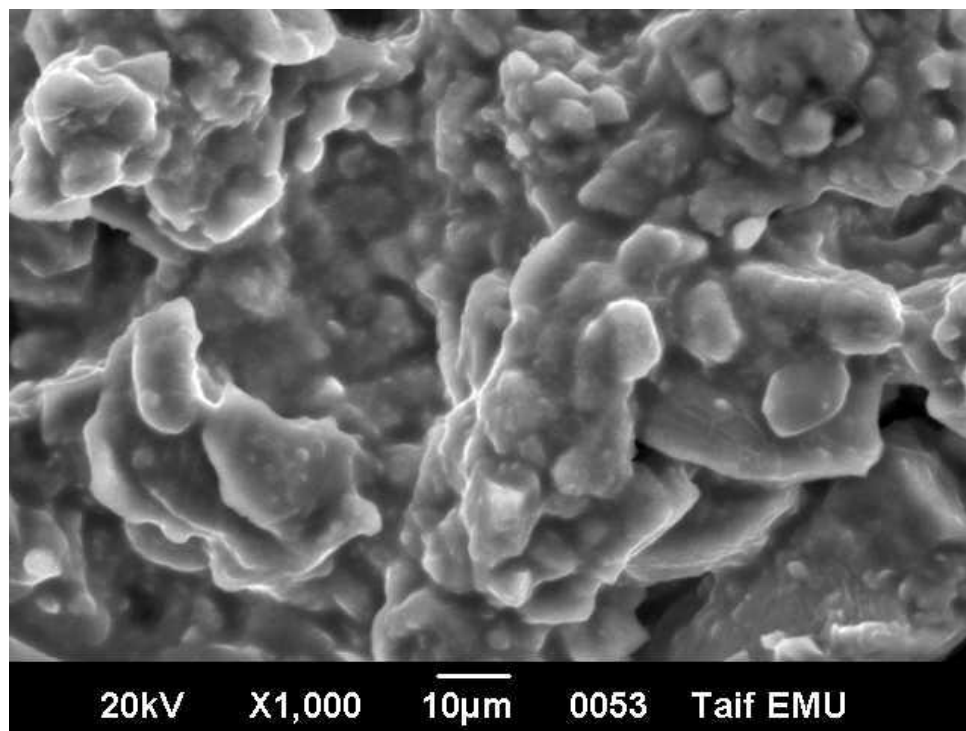
**Table 7**

Antibacterial and antifungal activity of HMDA and its synthesized CT complexes.

Sample	Inhibition zone diameter in mm at 100 µg/ml					
	Bacteria strains				Fungi strains	
	<i>Bacillus subtilis</i> , (G <sup>+</sup> ) <sup>a</sup>	<i>Escherichia coli</i> , (G <sup>-</sup> )	<i>Pseudomonas aeruginosa</i> , (G <sup>-</sup> )	<i>Staphylococcus aureus</i> , (G <sup>+</sup> )	<i>Aspergillus flavus</i>	<i>Candida albicans</i>
DMSO (control)	0.0	0.0	0.0	0.0	0.0	0.0
Tetracycline (Antibacterial agent)	34.0	32.0	34.0	30.0	-	-
Amphotericin B (Antifungal agent)	-	-	-	-	18.0	19.0
HMDA	5.0	4.0	5.0	6.0	0.0	0.0
[(HMDA)(QL)]	22.0	25.0	26.0	24.0	17.0	18.0
[(HMDA)(PA) <sub>2</sub> ]	9.0	10.0	9.0	9.0	0.0	0.0
[HMDA]·2Br <sub>2</sub>	11.0	9.0	12.0	9.0	0.0	0.0
[HMDA-I] <sup>+</sup> I <sub>3</sub> <sup>-</sup>	10.0	10.0	10.0	10.0	0.0	0.0
[(HMDA)(SnCl <sub>4</sub> )]	17.0	20.0	23.0	19.0	0.0	0.0
[(HMDA)(ZnCl <sub>2</sub> )]	13.0	12.0	14.0	13.0	0.0	0.0

<sup>a</sup> G: Gram reaction.

## Graphical Abstract



The interesting morphology of [HMDA]·2Br<sub>2</sub> complex

**Highlights**

- Six new charge-transfer complexes of hexamethylenediamine were reported.
- The complex containing the QL acceptor exhibited a remarkable electronic spectrum.
- The complex containing the bromine acceptor exhibited a remarkable morphology feature.

ACCEPTED MANUSCRIPT